Supporting information for:

Slow magnetic relaxation in octahedral low-spin Ni(III) complexes

Indrani Bhowmick, Andrew J. Roehl, James R. Neilson, Anthony K. Rappé, Matthew P. Shores*
Department of Chemistry, Colorado State University, Fort Collins, Colorado 80523-1872

Contents

Experimental Section

Preparations of compounds

All reactions were performed in air at ambient temperatures. All reagents, including cyclam (1, 4, 8, 11-tetraaza-cyclotetradecane), and metal salts, were purchased from commercial sources and used without further purification. Deionized water was used as the solvent for all reactions.

[Ni(cyclam)$(NO_3)_2$](NO_3) (1·NO_3). This compound was made by modification of a published method,[1] so as to isolate single crystals. Here, an aqueous solution (1 mL) of $Ni(NO_3)_2·6H_2O$ (73 mg, 0.25 mmol) was added to an aqueous solution (2 mL) of cyclam (50 mg, 0.25 mmol) and the solution was stirred for 2 hours. Concentrated HNO_3 (2 mL) was added to form a green solution. The solution was allowed to evaporate slowly in a 20 mL scintillation vial. Green rectangular crystals suitable for single crystal X-ray diffraction analyses were collected via filtration after 1 day, affording 86 mg of product (78% yield based on cyclam). IR (ATR): $\nu_{N\text{-}H}$ 3189; $\nu_{N\text{-}O}$ 1414, 1487, 1648 cm^{-1}. Absorption spectrum (H_2O): λ_{max} (ε_M in $M^{-1}·cm^{-1}$) 309 (8320), 355 (5850) and 547 (70) nm. Diffuse reflectance ($BaSO_4$ background): λ_{max} 201, 313, 371 and 732 nm. Anal. Calcd for $C_{10}H_{24}N_7NiO_9$ (FW = 445.05 g/mol): C, 26.99; H, 5.44; N, 22.03. Found: C, 26.66; H, 5.72; N, 22.15.

[Ni(cyclam)$(ClO_4)_2$]. This compound was synthesized according to literature methods[2,3] as the precursor of compounds **1·ClO4** and **2·ClO_4**, but was not recrystallized. Here, a solution of $Ni(ClO_4)_2·6H_2O$ (366 mg, 1.0 mmol) in 3 mL of ethanol was added slowly to a solution of cyclam (200 mg, 1.0 mmol) in 4 mL of ethanol in a 20 mL scintillation vial; the mixture was stirred for 30 minutes. The resulting orange precipitate was collected by filtration (417 mg, 91% yield assuming formula Ni(cyclam)$(ClO_4)_2$). The compound was used as isolated without any further purification. Anal. Calcd for $C_{10}Cl_2H_{24}N_4NiO_8$ (FW = 457.92 g/mol): C, 26.23; H, 5.28; N, 12.24. Found: C, 26.84; H, 5.24; N, 12.17.

[Ni(cyclam)$(NO_3)_2$](ClO_4) (1·ClO_4). This compound was synthesized according to a modification of the literature method,[4] where room temperature nitric acid was used instead of hot nitric acid. A 20 mL scintillation vial was charged with solid [Ni(cyclam)$(ClO_4)_2$] (50 mg, 0.11 mmol) and ca. 2 mL of concentrated nitric acid, resulting in a dark green solution. The solution was kept covered in a laboratory refrigerator (T ≈ –15 ºC), and dark green crystals were collected by filtration after one day, affording 38 mg of product (72% yield based on [Ni(cyclam)$(ClO_4)_2$]. IR (ATR): $\nu_{N\text{-}H}$ 3191; $\nu_{N\text{-}O}$ 1425, 1441, 1648, 1658; $\nu_{Cl\text{-}O}$ 1031, 1068, 1088 cm^{-1}. Diffuse reflectance ($BaSO_4$ background): λ_{max} 202, 308, 374 and 718 nm. Anal. Calcd for $C_{10}ClH_{24}N_6NiO_{10}$ (FW = 482.48 g/mol): C, 24.89; H, 5.01; N, 17.42. Found: C, 25.16; H, 5.00; N, 17.52.

[Ni(cyclam)$(NCS)_2$](ClO_4) (2·ClO_4). This compound was prepared by modification of a published method using $Na_2S_2O_8$ instead of ammonium persulphate.[1] An aqueous solution (~0.5 mL) of $Na_2S_2O_8$ (47.62 mg, 0.2 mmol) was added to an aqueous solution (4 mL) of Ni(cyclam)$(ClO_4)_2$ (45.77 mg, 0.1 mmol) in a 20 mL scintillation vial, and the resulting green solution was stirred for 30 minutes. After adding a solution of 85 mg of NaSCN dissolved in a minimum volume (ca. 0.5 mL) of water, the resulting brown solution was allowed to evaporate slowly in a 20 mL scintillation vial. Dark brown crystals suitable for X-ray diffraction were collected by filtration after one day, affording 32 mg of product (67% based on Ni(cyclam)$(ClO_4)_2$ precursor). IR (ATR): $\nu_{N\text{-}H}$ 3139, 3183; $\nu_{Cl\text{-}O}$ 1031, 1042, 1080, $\nu_{S\text{-}C\equiv N}$ 2059 cm^{-1}. Absorption spectrum (H_2O): λ_{max} (ε_M in $M^{-1}·cm^{-1}$) 291 (8320), 356 (2690) and 700 (40) $M^{-1}·cm^{-1}$ nm. Diffuse reflectance ($BaSO_4$ background): λ_{max} 196, 476, 620 and 998 nm. Anal. Calcd for $C_{12}H_{24}ClN_6NiO_4S_2$ (FW = 474.65 g/mol): C, 30.37; H, 5.10; N, 17.71. Found: C, 30.63; H, 5.03; N, 17.60.

Caution! Perchlorate salts are potentially explosive and should be handled in small quantities.

[Ni(cyclam)$(NO_3)_2$](NO_3)·2HNO_3 (3a). The preparation is similar to that performed for **1·NO_3**, albeit with additional heating. Solid $Ni(NO_3)_2·6H_2O$ (73 mg, 0.25 mmol) was added slowly to an aqueous solution (2 mL) of cyclam (50 mg, 0.25 mmol) in a 20 mL scintillation vial, followed by 3 hours of stirring at 50 ˚C, keeping the vial loosely covered. The solution was cooled to room temperature and 2 mL of concentrated HNO_3 was added, resulting in a green solution. Green block crystals suitable for single crystal X-ray diffraction were collected by filtration after 2 days, affording 101 mg of product (71% based on cyclam). IR (ATR): $\nu_{N\text{-}H}$ 3234; $\nu_{N\text{-}O}$ 1402, 1501, 1646 cm^{-1}. Absorption spectrum (H_2O): λ_{max} (ε_M in $M^{-1}·cm^{-1}$) 307 (8300), 360 (5850) and 551 (40) nm. Diffuse reflectance ($BaSO_4$ background): λ_{max} 201, 313, 371 and 714 nm. Anal. Calcd for $C_{10}H_{26}N_9NiO_{15}$ (FW

= 571.11 g/mol): C, 21.03; H, 4.59; N, 22.07 Found: C, 21.20; H, 4.33; N, 22.13. The overlap of the powder and single crystal X-ray diffraction data simulation further supports bulk purity of **3a** (Fig. S36).

$[Ni_{0.5}Co_{0.5}(cyclam)(NO_3)_2](NO_3)\cdot 2HNO_3$ (3b). An aqueous solution (1 mL) of $Ni(NO_3)_2\cdot 6H_2O$ (37 mg, 0.125 mmol) and $Co(NO_3)_2\cdot 6H_2O$ (37 mg, 0.125 mmol) was added to an aqueous solution (2 mL) of cyclam (50 mg, 0.25 mmol) in a 20 mL scintillation vial. The resulting mixture containing a green precipitate was warmed to 50 ˚C and was stirred for 3 hours, keeping the vial loosely covered, resulting in a transparent brown solution. The solution was cooled to room temperature. After adding 2 mL of concentrated HNO_3, the solution colour turned green. Slow evaporation of the solution (2 days) afforded small block green-brown crystals suitable for single crystal X-ray diffraction. The product was collected via filtration to yield 95 mg of green crystals (67% based on cyclam). IR (ATR): $\nu_{N\text{-}H}$ 3246; $\nu_{N\text{-}O}$ 1404, 1515, 1657 cm^{-1}. Anal. Calcd for $C_{10}H_{26}Co_{0.5}N_9Ni_{0.5}O_{15}$ (FW = 571.21 g/mol): C, 21.03; H, 4.59; N, 22.07 Found: C, 21.25; H, 4.38; N, 22.25. Absorption spectrum (H_2O): λ_{max} (ε_M in $M^{-1}\cdot cm^{-1}$) 305 (5030), 360 (3270) and 550 (30) nm. The absorption spectrum (Fig. S18) compares well to a simulated spectrum assuming a 1:1 ratio of absorption spectra of compounds **3a** and **3e**. Diffuse reflectance ($BaSO_4$ background): λ_{max} 201, 259, 306, 371, 573 and 747 nm.

$[Ni_{0.25}Co_{0.75}(cyclam)(NO_3)_2](NO_3)\cdot 2HNO_3$ (3c). This was prepared by the procedure used for **3b**, using 18 mg of $Ni(NO_3)_2\cdot 6H_2O$ (0.0625 mmol) and 55 mg of $Co(NO_3)_2\cdot 6H_2O$ (0.1875 mmol), to yield 95 mg of green crystals (67% based on cyclam). IR (ATR): $\nu_{N\text{-}H}$ 3238; $\nu_{N\text{-}O}$ 1402, 1514, 1656 cm^{-1}. Anal. Calcd for $C_{10}H_{26}Co_{0.75}N_9Ni_{0.25}O_{15}$ (FW = 571.26 g/mol): C, 21.03; H, 4.59; N, 22.07 Found: C, 20.08; H, 4.24; N, 21.86. Absorption spectrum (H_2O): λ_{max} (ε_M in $M^{-1}\cdot cm^{-1}$) 305 (3200), 360 (2100) and 554 (25) nm. A comparison of the absorption spectrum with a simulated spectrum using the absorption spectra of compounds **3a** and **3e** indicates an approximately 3:1 ratio of Co(III) and Ni(III) in **3c** (Fig. S18); but this comparison is less precise in **3c** compared to the other mixed metal compounds. As we did not perform the magnetic measurement for **3c**, we did not attempt to quantify further the exact ratio of metal ions. Diffuse reflectance ($BaSO_4$ background): λ_{max} 201, 259, 306, 373, 575 and 754 nm.

$[Ni_{0.1}Co_{0.9}(cyclam)(NO_3)_2](NO_3)\cdot 2HNO_3$ (3d). This was prepared by the procedure used for **3b**, using 7.3 mg of $Ni(NO_3)_2\cdot 6H_2O$ (0.025 mmol) and 66 mg of $Co(NO_3)_2\cdot 6H_2O$ (0.225 mmol), affording 97 mg of greenish brown crystals suitable for X-ray diffraction (68% based on cyclam). IR (ATR): $\nu_{N\text{-}H}$ 3234; $\nu_{N\text{-}O}$ 1401, 1509, 1654 cm^{-1}. Anal. Calcd for $C_{10}H_{26}Co_{0.9}N_9Ni_{0.10}O_{15}$ (FW = 571.30 g/mol): C, 21.03; H, 4.59; N, 22.07 Found: C, 21.03; H, 4.46; N, 21.97. Absorption spectrum (H_2O): λ_{max} (ε_M in $M^{-1}\cdot cm^{-1}$) 363 (757) and 551 (58) nm. The absorption spectra compares well with a simulated spectrum using a 9:1 ratio of the absorption spectra of compounds **3a** and **3e** (Fig. S18). Diffuse reflectance ($BaSO_4$ background): λ_{max} 201, 259, 306, 374, 576 and 754 nm.

$[Co(cyclam)(NO_3)_2](NO_3)\cdot 2HNO_3$ (3e). This was prepared by the procedure used for **3a**, using 73 mg of $Co(NO_3)_2\cdot 6H_2O$ (0.25 mmol), to yield 93 mg of brown crystals (66% based on cyclam). IR (ATR): $\nu_{N\text{-}H}$ 3241; $\nu_{N\text{-}O}$ 1411, 1514, 1653 cm^{-1}. Anal. Calcd for $C_{10}H_{26}CoN_9O_{15}$ (FW = 571.30 g/mol): C, 21.02; H, 4.59; N, 22.07. Found: C, 21.10; H, 4.44; N, 21.96. The solution electronic absorption spectrum (H_2O) does not show significant peaks at wavelengths greater than 350 nm (Fig. S18). Diffuse reflectance ($BaSO_4$ background): λ_{max} 201, 261, 305, 437 and 577 nm. We note that a synthetically-distinct preparation of a related $[Co(cyclam)(NO_3)_2](NO_3)\cdot HNO_3$ compound has been reported:[5] that compound contains only one HNO_3 molecule per complex. The literature synthetic method is very different from us which used $[Co(cyclam)Cl_2]Cl$ precursor, $AgNO_3$ and concentrate nitric acid, that shows co-crystallization of nitric acid is not unusual in these type of systems.

Magnetic measurements

All magnetic susceptibility measurements were performed with a Quantum Design MPMS-XL SQUID magnetometer. Microcrystalline samples of all compounds and aqueous solutions of **$1\cdot NO_3$** were loaded into 1 cm × 1.5 cm polyethylene bags and sealed, inserted into plastic straws, and transported to the SQUID magnetometer under dinitrogen. Ferromagnetic impurities were checked through a variable field analysis of magnetization at 100 K: no significant impurities were detected (Fig. S8). Data were corrected for the magnetization of the sample holder; diamagnetic corrections of the sample were applied using Pascal's constants.[6] Solid state magnetic susceptibility measurements

were performed between 1.8 K and 300 K under 1000 Oe dc applied fields. Measurements of flash-frozen aqueous solutions were performed between 1.8 K and 220 K. Magnetization data were collected between 0 Oe and 50 kOe in the temperature range 2 K - 20 K. Dynamic (ac) magnetic susceptibility measurements were performed on samples at temperatures 1.8 K - 30 K with an oscillating field of 4 Oe in the frequency range 0.1 Hz - 1500 Hz.

Other physical methods

Infrared spectra were measured with a Nicolet 380 FT-IR spectrometer under a dinitrogen flow, using an ATR attachment with a ZnSe crystal in the range 400 cm^{-1} - 4000 cm^{-1}. Absorption spectra were obtained with a Hewlett-Packard 8453 spectrophotometer in quartz cuvettes with 1 cm path lengths; all experiments were performed at room temperature. Diffuse reflectance data were obtained with a Thermo Scientific Evolution 300 UV-Vis spectrophotometer, using $BaSO_4$ for background. The X-band EPR studies on powdered samples and flash-frozen aqueous solutions were performed at 100 K with a Bruker ESR-300 spectrometer. The XPS measurements were done with a PE-5800 X-ray photoelectron spectrometer, using an Al Kα X-ray source (1486.6 eV); high resolution scans were performed between 852 eV and 887 eV, with a passing energy of 23.5 eV and 0.1 eV/step. Powder X-ray diffraction data were collected at room temperature using a Scintag X-2 powder X-ray diffractometer equipped with Cu Kα radiation, scintillation detector and stationary sample stage between 5° and 70° 2θ. Rietveld analysis was performed using the GSAS/EXPGUI code[22] using an instrument parameter file defined by polycrystalline Si. Elemental analyses were performed by Robertson Microlit Laboratories, Inc. in Madison, NJ.

Single crystal X-ray structure determinations

Crystals suitable for X-ray analysis were coated with Paratone-N oil and supported on a Cryoloop before being mounted on a Bruker Kappa Apex II CCD diffractometer under a stream of dinitrogen. Data collections were performed at 120 K with Mo-Kα radiation (λ = 0.71073 Å) and a graphite monochromator, targeting complete coverage and 4-fold redundancy. Crystallographic data and metric parameters are presented in Table S1. Integrations of the raw data were done using the Apex II software package and absorption corrections were applied using SADABS.[7] The structures were solved by direct methods and refined against F^2 with SHELXS-2013 using the WINGX-2014 software package.[8] Thermal parameters for all non-hydrogen atoms were refined anisotropically. Hydrogen atoms were added at the ideal positions and were refined using a riding model, with thermal parameters set at 1.2 times those of the bound carbon atoms (1.5 for methyl groups). For the structure of **3**, the H atoms for the interstitial nitric acid molecules were not calculated in the crystal structure, but they were included to calculate the total molecular weight.

Table S1. Crystallographic data for compounds [Ni(cyclam)$(NO_3)_2$](NO_3) (**1·NO_3**), Ni(cyclam)$(NCS)_2$](ClO_4) (**2·ClO_4**), [Ni(cyclam)$(NO_3)_2$](NO_3)·2HNO_3 (**3a**), and [$Ni_{0.1}Co_{0.9}$(cyclam)$(NO_3)_2$](NO_3)·2HNO_3 (**3d**)

	1·NO_3	**2·ClO_4**	**3a**	**3d**
formula	$C_{10}H_{24}N_7NiO_9$	$C_{12}H_{24}ClN_6NiO_4S_2$	$C_{10}H_{26}N_9NiO_{15}$	$C_{10}H_{26}Co_{0.9}N_9Ni_{0.10}O_{15}$
CCDC number	1579276	1579279	1579280	1579281
fw (g/mol)	445.05	474.65	571.11	571.30
color, habit	green, block	brown, block	green, block	brown, block
T, K	120	120	120	120
λ, Å	0.71073	0.71073	0.71073	0.71073
crystal system	Monoclinic	Triclinic	Triclinic	Triclinic
space group	*C*2/*c*	$P\bar{1}$	$P\bar{1}$	$P\bar{1}$
Z	4	2	2	1
a, Å	12.8157(8)	7.59(6)	7.4549(13)	7.371(5)
b, Å	8.8179(5)	8.72(7)	9.0814(16)	8.496(4)
c, Å	15.3168(9)	15.75(12)	16.935(3)	9.080(5)
α, deg	90	83.72(9)	88.505(7)	89.163(3)
β, deg	106.818(2)	81.37(9)	81.132(7)	76.951(5)
γ, deg	90	80.39(11)	76.008(7)	81.894(4)
V, Å	1656.88(17)	1013(14)	1099.1(3)	548.3(5)
d_{calc} (g/cm^3)	1.784	1.560	1.726	1.724
μ, mm^{-1}	1.238	1.327	0.976	0.886
F(000)	932	494	594	294
crystal size (mm^3)	0.06×0.04×0.04	0.10×0.10×0.04	0.04×0.04×0.02	0.04×0.04×0.02
reflections	2463	3401	5365	2728
GOF	1.063	1.017	1.100	1.187
completeness, %	98.6	94.4	98.9	99.8
R_1[a] (wR_2)[b],% (I>2σ(I))	2.06 (5.31)	6.51 (14.23)	3.37 (8.78)	3.55 (10.08)
R indices (all data)	2.31 (5.43)	9.83 (15.87)	5.49 (12.41)	4.08 (11.80)

[a] $R_1 = \Sigma||F_o| - |F_c||/ \Sigma |F_o|$.

[b] $wR_2 = [\Sigma [w(F_o^2-F_c^2)^2]/ \Sigma [w(F_o^2)^2]]^{½}$, $w = 1/[\sigma^2(F_o^2) + (aP)^2 + bP]$, where $P = [\max(F_o^2 \text{ or } 0) + 2(F_c^2)]/3$

Table S2. Intra- and inter molecular hydrogen bonding interactions in compounds [Ni(cyclam)$(NO_3)_2$](NO_3) (**1·NO_3**), [Ni(cyclam)$(NO_3)_2$](NO_3) (**1·ClO_4**), Ni(cyclam)$(NCS)_2$](ClO_4) (**2·ClO_4**), [Ni(cyclam)$(NO_3)_2$](NO_3)·2HNO_3 (**3a**) [$Ni_{0.1}Co_{0.9}$(cyclam)$(NO_3)_2$](NO_3)·2HNO_3 (**3d**)

Compound	Intra-molecular			Inter-molecular		
	N-H···O	distance (Å)	angle (°)	N-H···O	distance (Å)	angle (°)
1·NO_3	N3-H3···O4	2.892(1)	147.1(1)	N2-H2···O2	3.012(1)	156.5(3)
1·ClO_4	N5-H14A···O6A	2.218(1)	159.4(1)	N4-H13···O8	2.926(2)	151.2(1)
	N2-H2A··· O2A	3.030(1)	136.5(2)	N1-H1···O7	2.977(1)	139.1(4)
2·ClO_4				N4-H4···O1	3.003(1)	139.3(1)
				N5-H5···S2	3.267(2)	149.1(1)
3a	N4-H4···O5	3.056(2)	130.5(4)	N2-H2···O6	2.936(3)	123.4(5)
	N3-H3···O5	3.024(3)	131.0(1)	N4-H4···O2	2.990(3)	121.5(1)
	N2-H2···O3	2.993(2)	135.7(5)			
3d	N1-H1···O1	2.964(2)	132.1(1)	N1-H1···O2	2.953(1)	129.7(1)
	N2-H2···O2	2.993(3)	128.6(2)			

Table S3. Unit cell parameters for the structures of compounds **3a-e**, collected at 120 K.

Compound	**3a***	**3b**	**3c**	**3d**	**3e**
Empirical formula	$C_{10}H_{26}NiN_9O_{15}$	$C_{10}H_{26}Co_{0.75}N_9Ni_{0.25}O_{15}$	$C_{10}H_{26}Co_{0.50}N_9Ni_{0.50}O_{15}$	$C_{10}H_{26}Co_{0.9}N_9Ni_{0.10}O_{15}$	$C_{10}H_{26}CoN_9O_{15}$
a (Å)	7.4549(13)	7.44(4)	7.55(4)	7.371(5)	7.44(4)
b (Å)	9.0814(16)	8.50(3)	8.61(4)	8.496(4)	8.68(3)
c (Å)	16.935(3)	9.10(4)	9.21(3)	9.080(5)	9.13(5)
α (˚)	88.505(7)	89.16(5)	89.13(5)	89.163(3)	89.33(5)
β (˚)	81.132(7)	76.76(3)	76.78(5)	76.951(5)	76.97(3)
γ (˚)	76.008(7)	82.26(5)	82.70(3)	81.894(4)	81.89(5)
V (Å^3)	1099.1(3)	556(4)	578(4)	548.3(5)	572(5)

* The c axis length is double that of the b axis of other isostructural compounds **3b-e**

Electronic Structure Calculations

The heavy atom crystal structure coordinates were used directly, C-H bond distances were lengthened to 1.09 Å. For the TD-DFT calculations[9] in g09/g16[10] the 6-311+g* basis[11] and B3LYP hybrid density functional[7] were used to obtain the ground state electronic wave functions. To account for the crystal lattice, a PCM continuum solvation model[12] was included. A stability check was carried out on the resulting wave functions to ensure that it was the lowest energy doublet.[9] Quartet states were also considered and found to be more than 20 kcal/mol above the doublet. The solvated 6-311+g* B3LYP total energies (in Hartrees) for **1·NO$_3$, 1·ClO$_4$**, and **2·ClO$_4$** are -2964.28065003, -3444.68514947, and -3866.14630008, respectively. For the computation of the *g* tensors, the ORCA suite of programs was used[13]. The EPR II basis[14] was used for the B3LYP computation while the NEVPT2[15] and SORCI[16] studies used the cc-pVDZ basis, with nickel described by a cc-pVTZ basis[17]. For the ORCA studies, a CPCM solvation model[18] was utilized.

Derivatives of *g* and *A* with respect to normal mode coordinate were obtained using finite differences of the property versus nuclear displacement. That is, the structure was diplaced along each of the normal modes in the plus and minus direction a fixed amount and the property recalculated. For the first derivatives the average of the plus and minus displaced values were used, and to estimate the second derivative the difference between the plus and minus displace values were used. For this study B3LYP was used with the EPR II basis.

Periodic, plane-wave DFT calculations were also performed on [Ni(cyclam)Br$_2$]Br using the Vienna Ab Initio Simulation Package (VASP[23]) with the B3LYP hybrid density functional[7] in both the ferromagnetic and antiferromagnetic spin configurations of the crystal (2 Ni per unit cell). A plane-wave basis set was used, with the interactions between core and valence electrons described using the Projector Augmented Wave (PAW) method.[24] In either case, the spin density was localized the the Ni and axial ligands, justifying the need for the continuum solvation model.

Data Deposited as Supporting Information

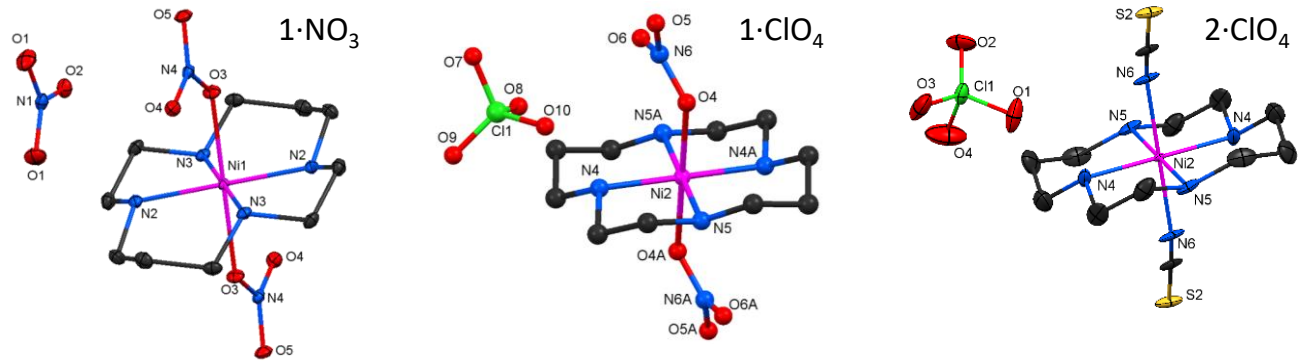

Figure S1. Crystal structures of compounds **1·NO$_3$, 1·ClO$_4$**[4] and **2·ClO$_4$.** Thermal ellipsoids are rendered at the 50 % probability level. Magenta, green, blue, red, black and yellow spheres represent the Ni, Cl, N, O and C atoms, respectively. Hydrogen atoms are omitted for clarity.

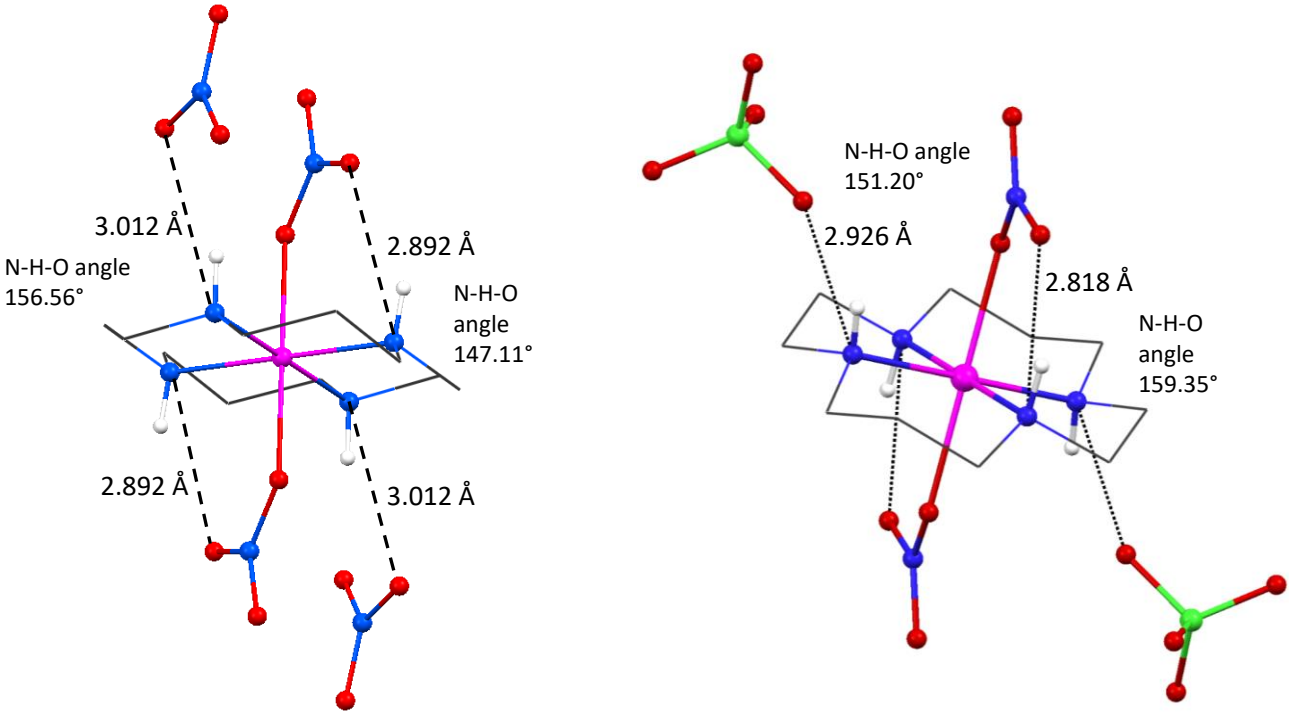

Figure S2. Intra- and inter molecular H-bonding interactions in the structures of **1·NO$_3$** and **1·ClO$_4$.**[4]

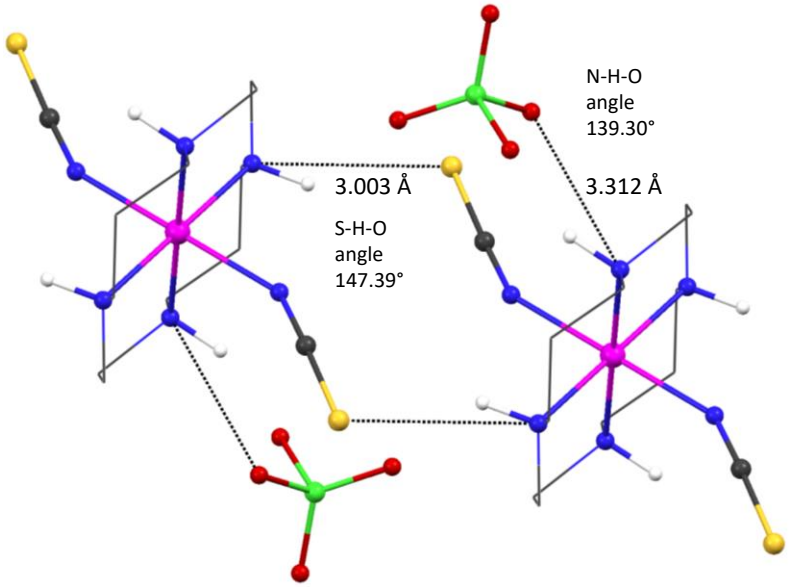

Figure S3. Inter molecular H-bonding interactions in the structure of **2·ClO$_4$**.

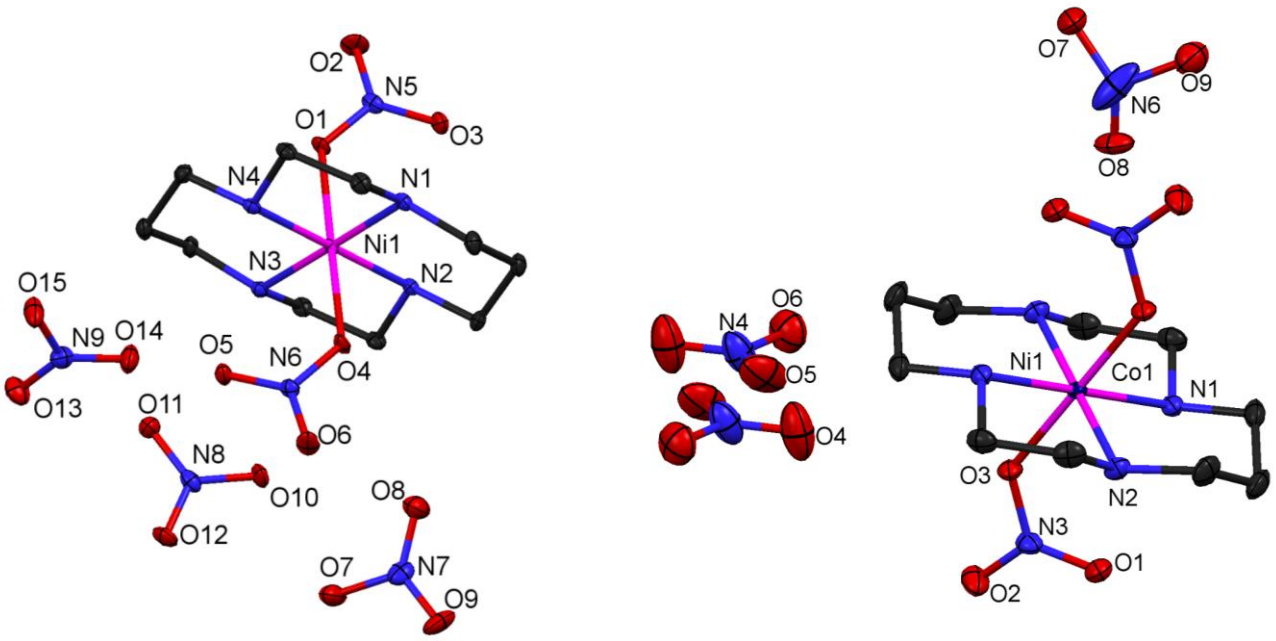

Figure S4. Crystal structures of compounds **3a** (left) and **3d** (right). Thermal ellipsoids are rendered at the 50% probability level. Magenta, blue, red and black ellipsoids represent the Ni, N, O and C atoms, respectively. The navy-blue ellipsoid represents the mixed metal site (10% Ni and 90% Co) in **3d**. Hydrogen atoms are omitted for clarity.

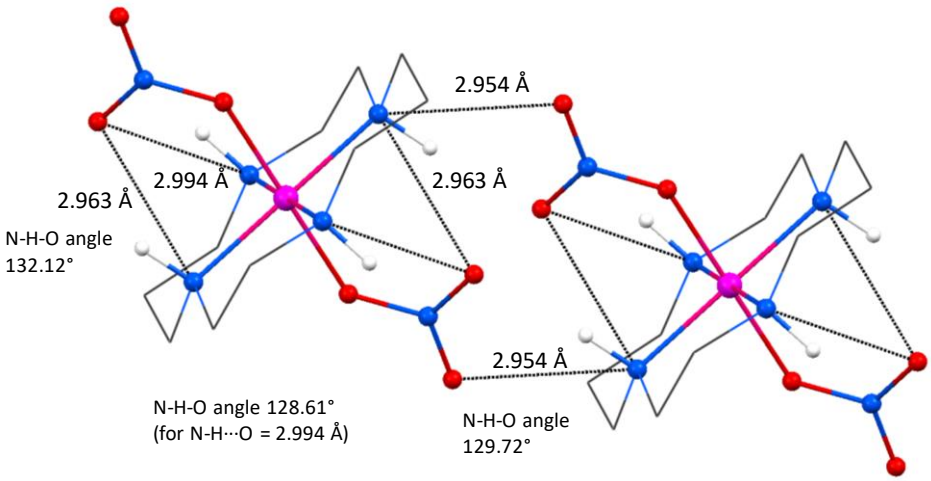

Figure S5. Intra- and inter-molecular H-bonding interactions in the structure of compound **3d.**

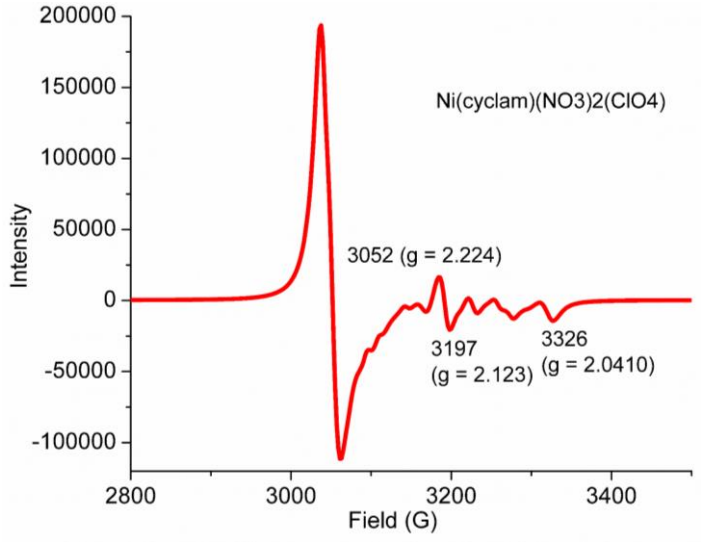

Figure S6. EPR spectrum of **1·ClO$_4$**, collected on a powdered crystalline sample at 100 K.

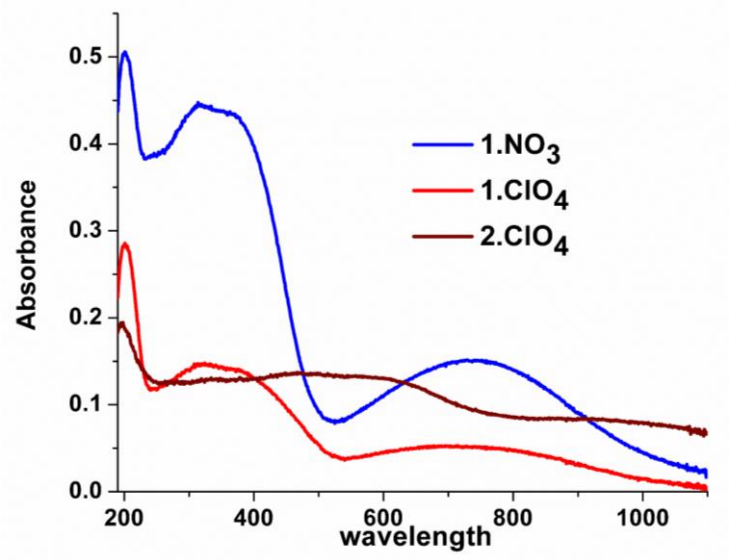

Figure S7. Diffuse reflectance spectral data for **1·NO$_3$**, **1·ClO$_4$** and **2·ClO$_4$**, collected with a $BaSO_4$ background.

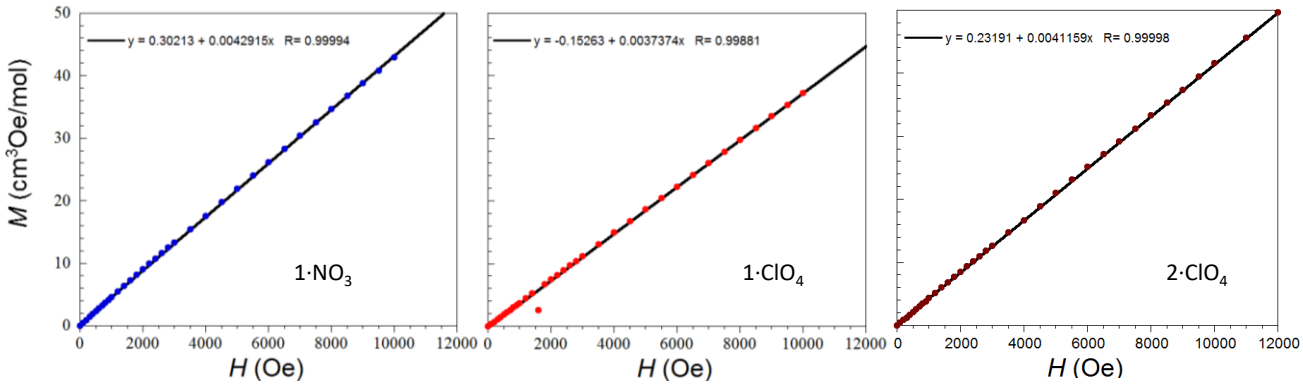

Figure S8. Plots of *M* vs. *H* for **1·NO$_3$, 1·ClO$_4$** and **2·ClO$_4$,** collected at 100 K. The linear fits of the data (solid black lines) indicate the absence of ferromagnetic impurities in these samples.

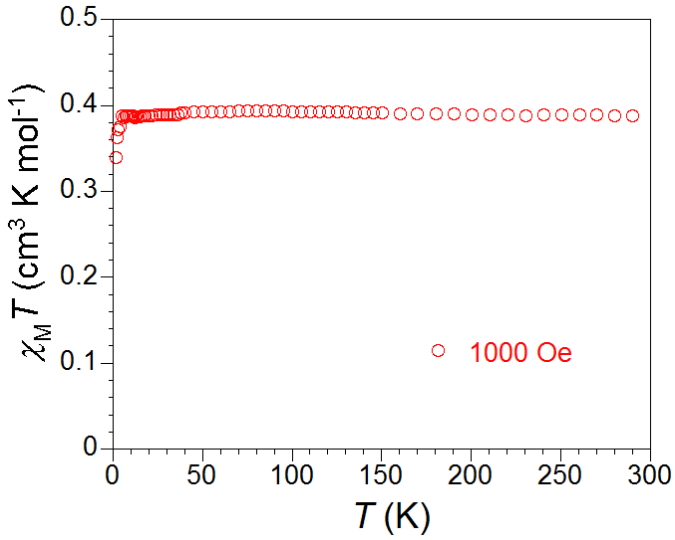

Figure S9. Temperature dependence of $\chi_M T$ for **1·ClO$_4$**, collected at 1000 Oe between 1.8 K and 300 K.

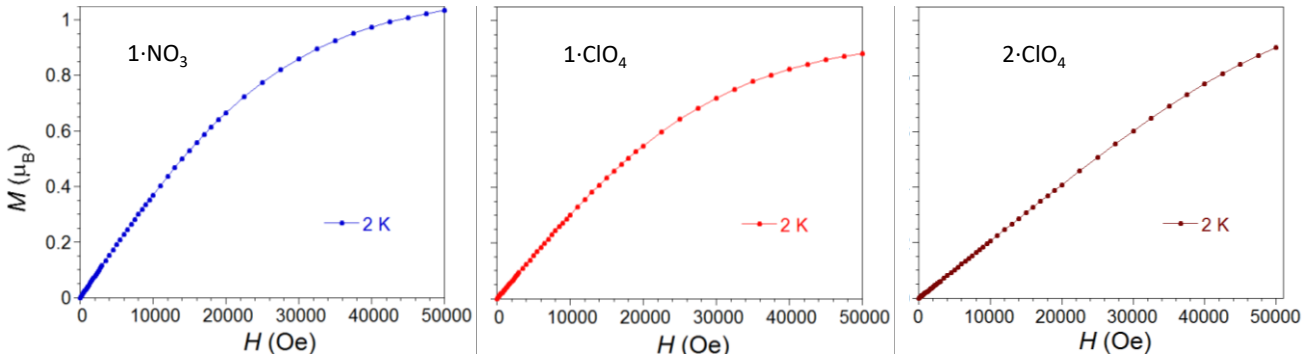

Figure S10. Field dependence of magnetization for **1·NO$_3$**, **1·ClO$_4$** and **2·ClO$_4$**, collected at 2 K between 0 Oe and 50 kOe. At 5 T, the data approach saturation near 1 μ_B, indicating the presence of only one unpaired electron per formula unit. For the perchlorate salts, the field dependences of magnetization data do not match the Brillouin function expected for a sample of noninteracting S = ½ ions.

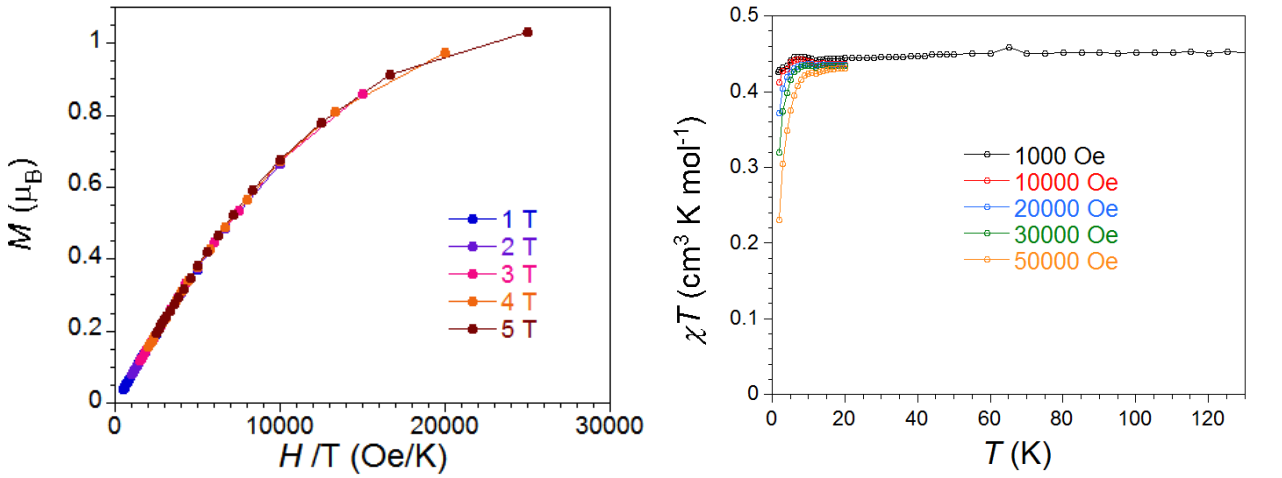

Figure S11. Left: dependence of magnetization on reduced field (H/T) for **1·NO$_3$**, collected at five different fields between 0 Oe and 50000 Oe, at temperatures between 2 K and 20 K. The isofield lines (guides to the eye) are mostly superimposed, consistent with lack of large axial magnetic anisotropy as expected for a S = ½ system. Right: $\chi_M T$ vs T plots for **1·NO$_3$**, collected at different fields between 0.1 T to 5 T, show that the small "hump" observed at low temperatures (below 12 K) persists up to 3 T.

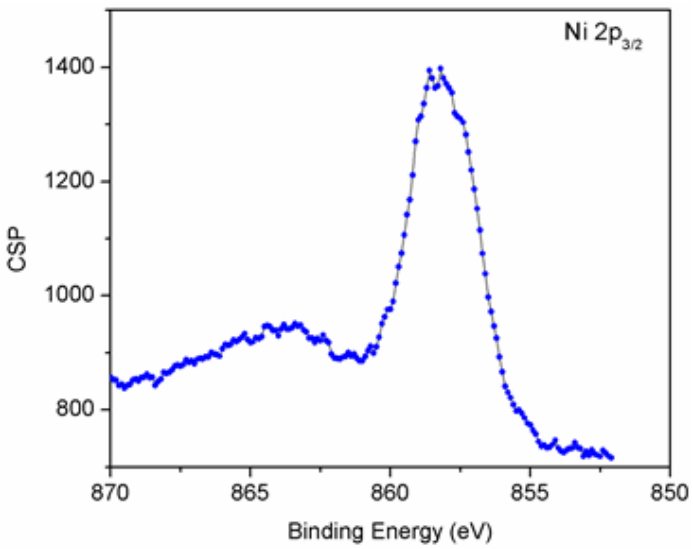

Figure S12. X-ray photoelectron (Ni $2p_{3/2}$) spectrum for **1·NO$_3$**. The ground state Ni^{3+} ion shows the surface peak at 858.4 eV.

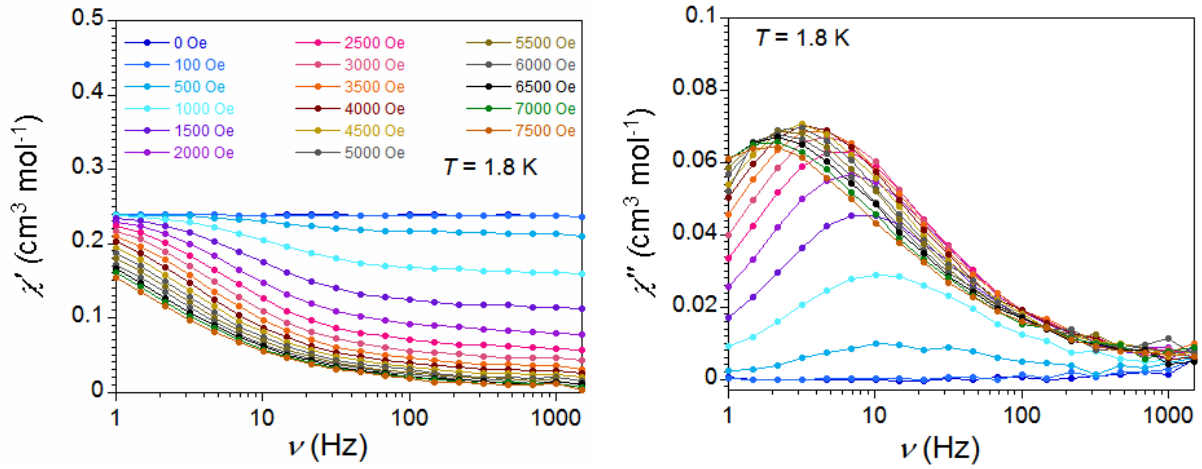

Figure S13. Frequency dependence of in-phase (χ') and out-of-phase (χ'') ac magnetic susceptibilities of **1·NO$_3$**, measured at 1.8 K at applied dc fields between 0 Oe and 7500 Oe, with a 4 Oe oscillating ac field.

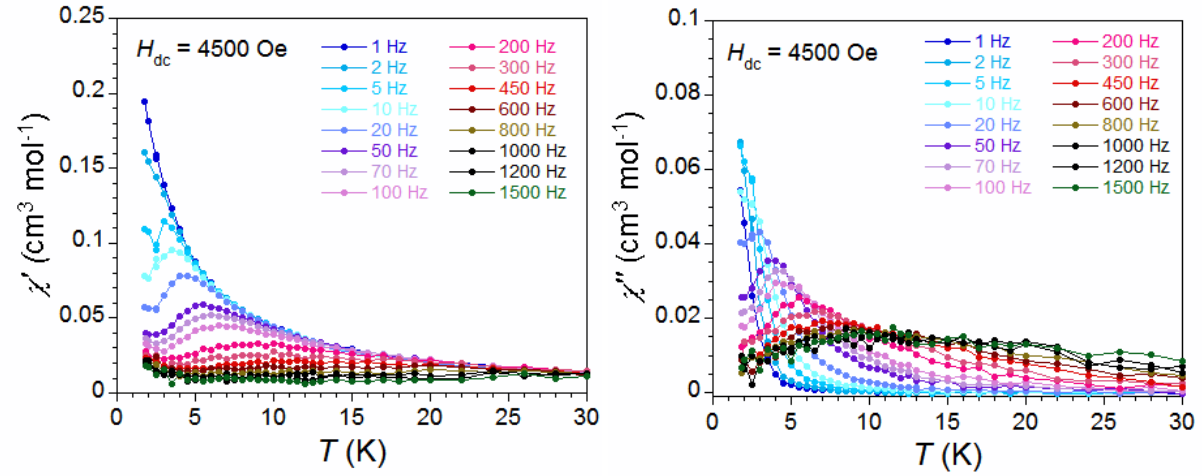

Figure S14. Temperature dependence of in-phase (χ') and out-of-phase (χ'') ac magnetic susceptibilities of **1·NO$_3$**, measured at different frequencies under an applied dc field of 4500 Oe, with a 4 Oe oscillating ac field.

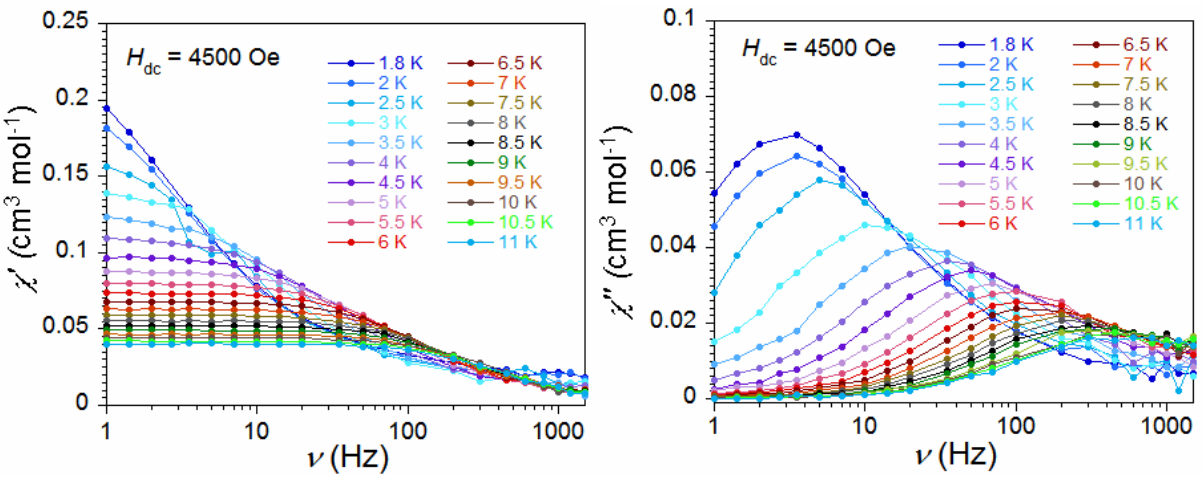

Figure S15. Frequency dependence of in-phase (χ') and out-of-phase (χ'') ac magnetic susceptibilities of **1·NO$_3$**, measured at different temperatures under an applied dc field of 4500 Oe**,** with a 4 Oe oscillating ac field.

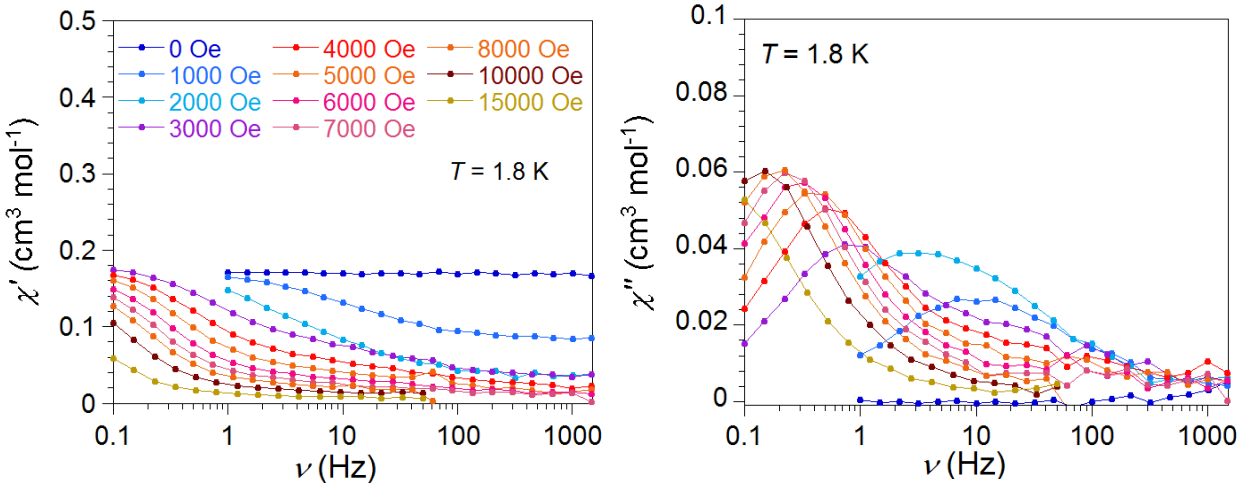

Figure S16. Frequency dependence of in-phase (χ') and out-of-phase (χ'') ac magnetic susceptibilities of **1·ClO$_4$**, measured at 1.8 K at applied dc fields between 0 Oe and 15000 Oe, with a 4 Oe oscillating ac field.

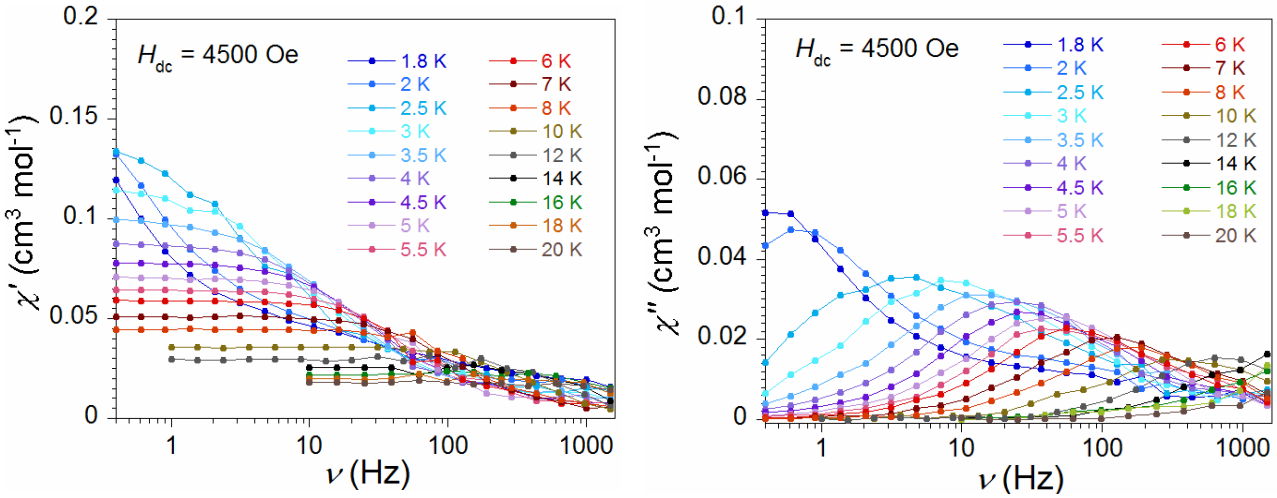

Figure S17. Frequency dependence of in-phase (χ') and out-of-phase (χ'') ac magnetic susceptibilities of **1·ClO$_4$**, measured at different temperatures under an applied dc field of 4500 Oe, with a 4 Oe oscillating ac field.

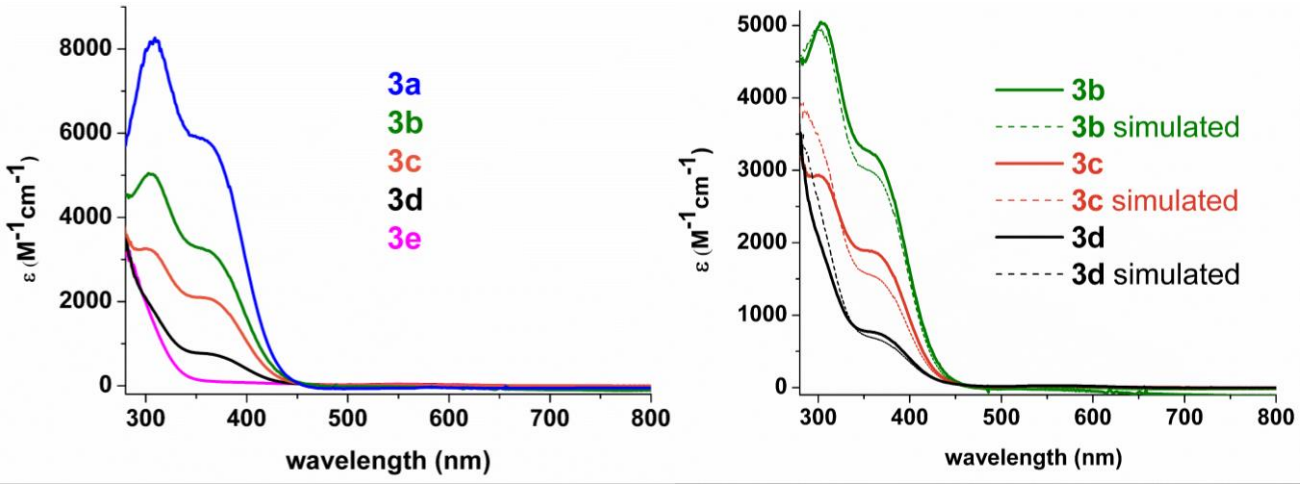

Figure S18. Left: Electronic absorption spectra for aqueous solutions of compounds **3a-e.** Right: comparison of the spectra of mixed metal complexes **(3b-d)** with the simulated spectra of **3a** (pure Ni(III) analogue) and **3e** (pure Co(III) analogue).

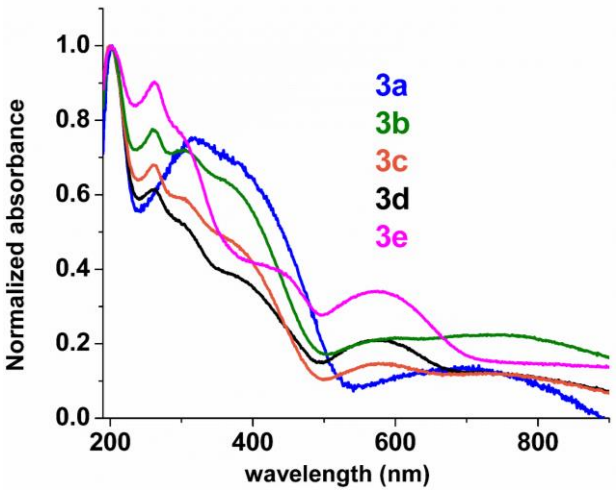

Figure S19. Diffuse reflectance spectral data for **3a-e**, collected with a $BaSO_4$ background. All data were normalized to maximum relative absorbance 1.0 by dividing the spectral absorbance values by the absorbance value at λ_{max} (~200 nm).

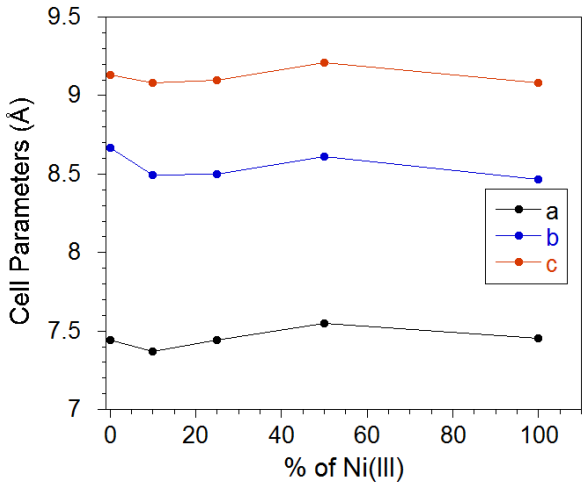

Figure S20. Dependence of unit cell parameters on the relative amount of Ni(III) present in compounds **3b-e.**

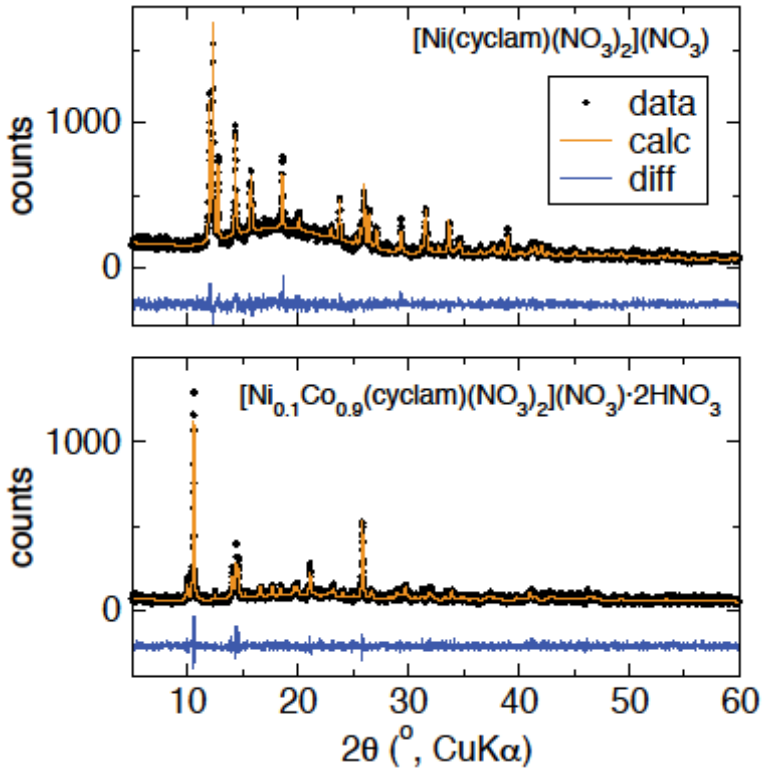

Figure S21. Powder X-ray diffraction (PXRD) data for **1·NO$_3$** (top) and **3d** (bottom) and comparison to the simulations from single crystal X-ray diffraction data using the Rietveld method (orange line, calc). Data are shown as black circles; and difference curves are shown below as blue lines.

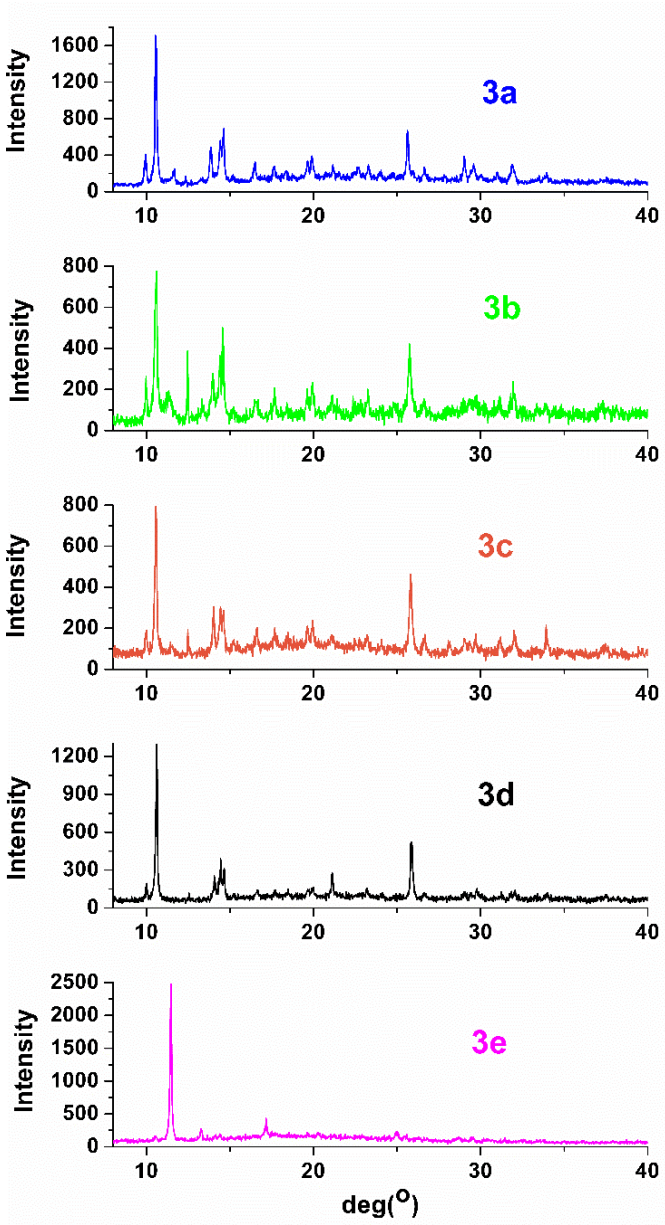

Figure S22. Powder X-ray diffraction (PXRD) data for members of the solid solution **3a-3e.** To clarify, the x-axis is marked off in degrees 2θ (i.e. standard formatting). Note that the ratio of intensities for the peaks at ~10° 2θ and 14-15° 2θ shifts higher as the mole fraction of Co increases.

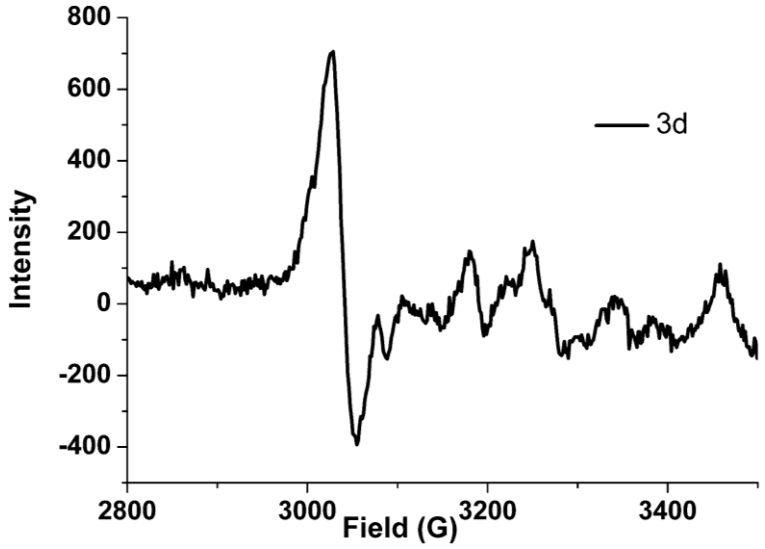

Figure S23. X-band EPR spectra of a powdered crystalline sample of **3d**, collected at 100 K, indicating the presence of S = ½ Ni(III) ions.

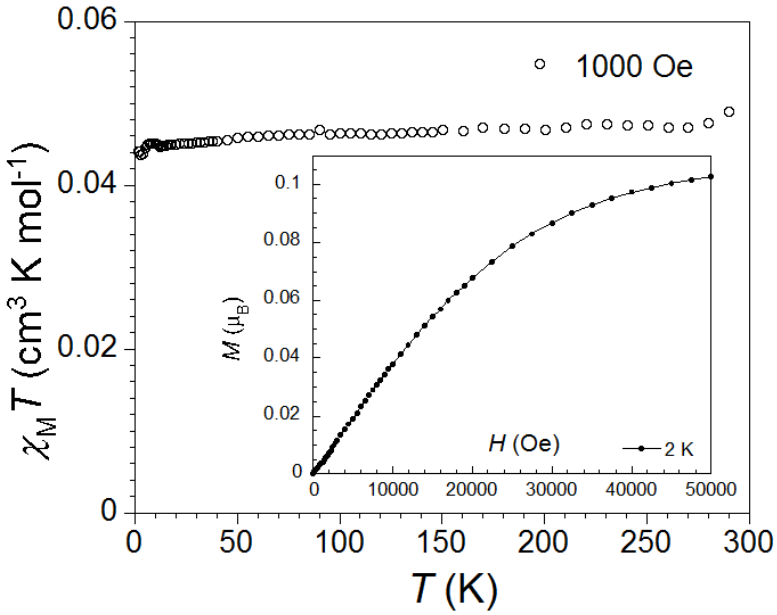

Figure S24. Temperature dependence of magnetic susceptibility for compound **3d**, measured at 1000 Oe in the temperature range 1.8 K - 300 K. Inset: a plot M vs H for 3d, collected at 2 K between 0 Oe and 50000 Oe. The molecular mass used is for the full compound, including the diamagnetic Co(III) component; thus, the values of $\chi_M T$ and H indicate 10% of the sample contains paramagnetic Ni(III) ions.

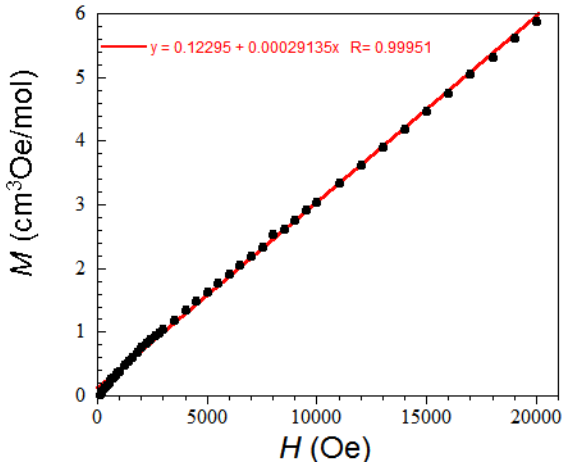

Figure S25. Plot of *M* vs. *H* for compound **3d**, collected at 100 K. The linear fit of the data (solid red line) indicates the absence of ferromagnetic impurities.

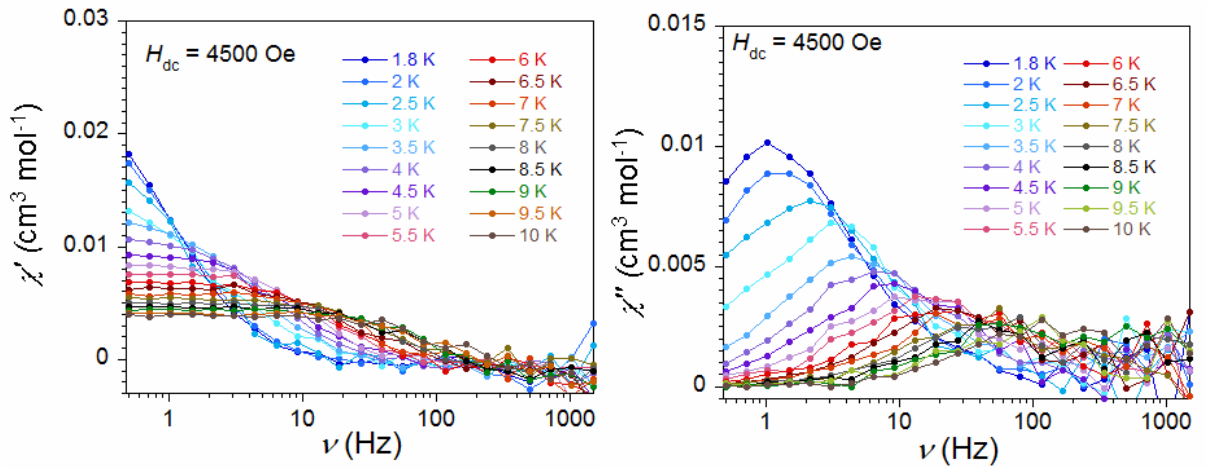

Figure S26. Frequency dependence of in-phase (χ′) and out-of-phase (χ″) ac magnetic susceptibilities for **3d** at different temperatures under an applied dc field of 4500 Oe, with a 4 Oe oscillating ac field.

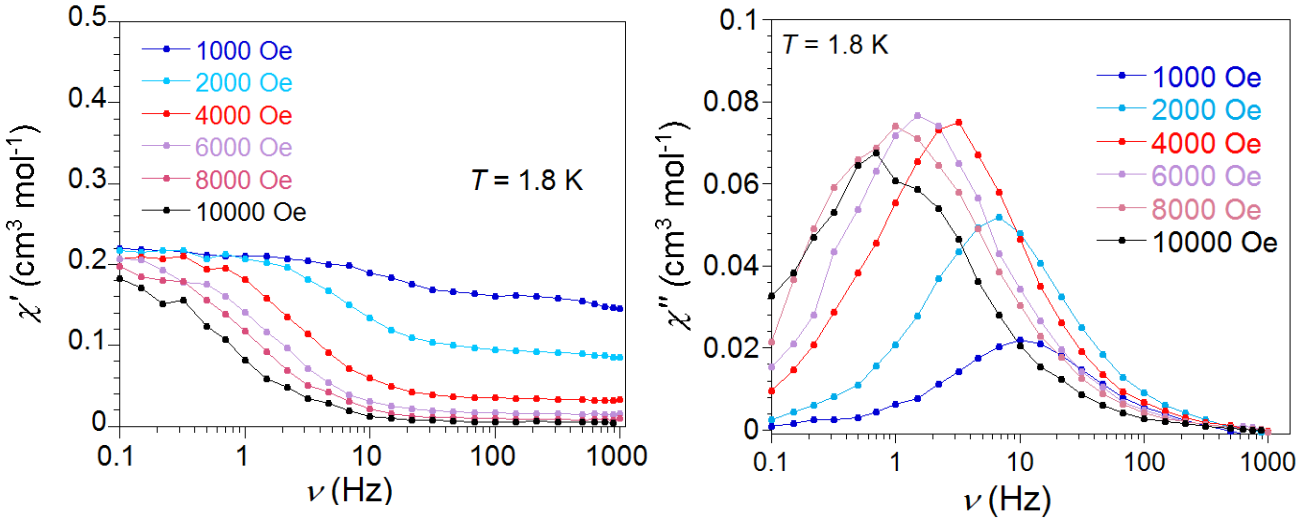

Figure S27. Frequency dependence of in-phase (χ') and out-of-phase (χ") ac magnetic susceptibilities of **3a**, measured at 1.8 K at different applied dc fields between 1 kOe and 10 kOe, with a 4 Oe oscillating ac field.

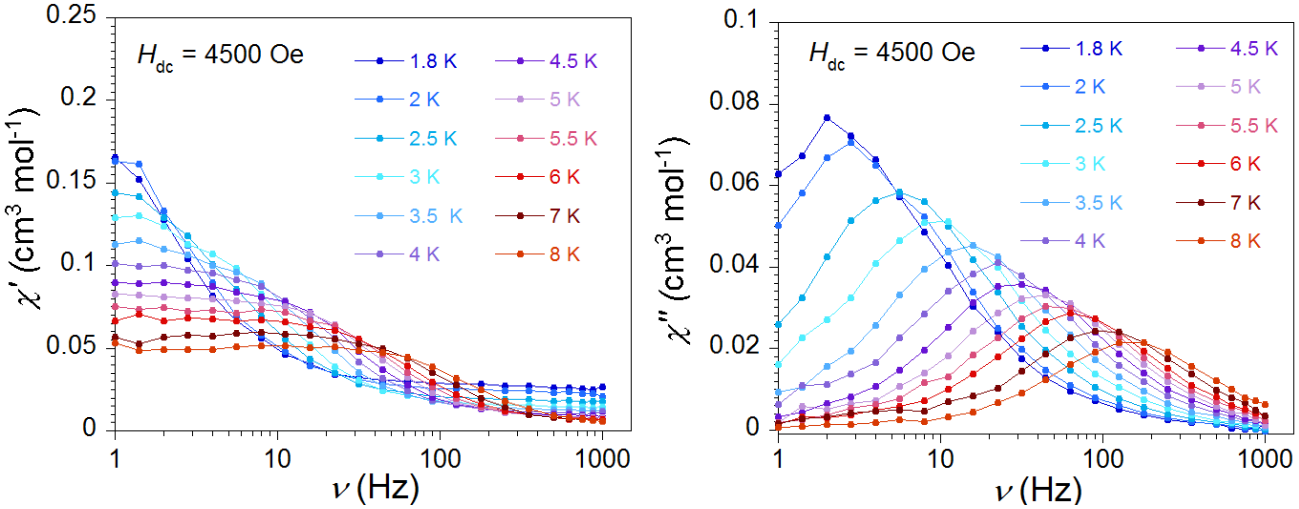

Figure S28. Frequency dependence of in-phase (χ') and out-of-phase (χ'') ac magnetic susceptibilities of **3a** at different temperatures under an applied dc field of 4500 Oe, with a 4 Oe oscillating ac field.

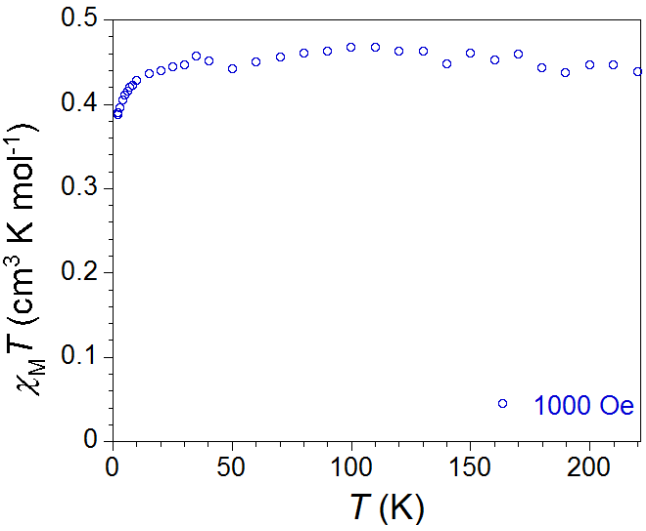

Figure S29. Plot of $\chi_M T$ vs. T data for **1·NO₃(aq)** (at concentration 8.8 × 10^{-2} M) measured at 1000 Oe in the temperature range 1.8 K - 220 K. The aqueous solution was flash-frozen in liquid N_2 before measuring.

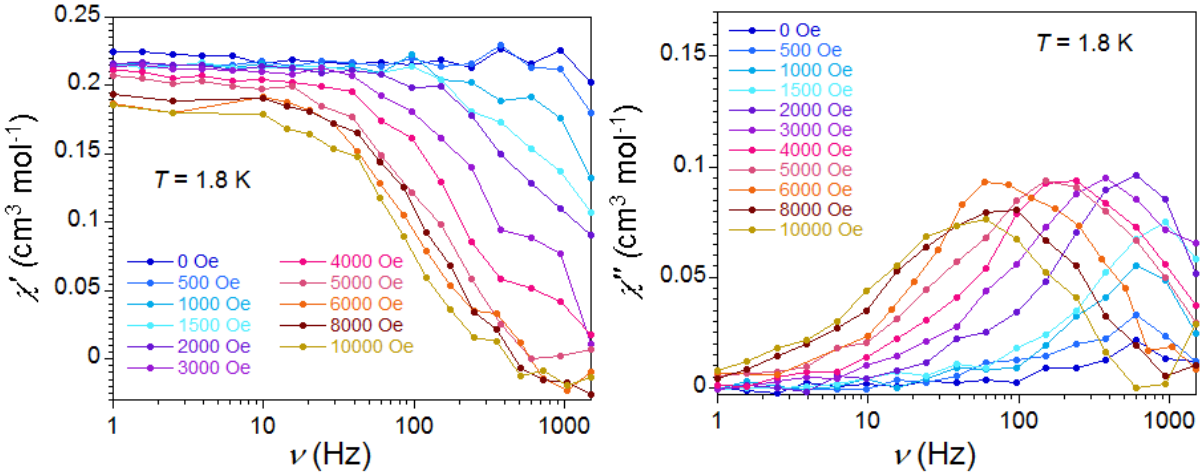

Figure S30. Static field dependence of ac susceptibility signal for **1·NO₃(aq).** Frequency dependence of in-phase (χ') and out-of-phase (χ'') ac magnetic susceptibility of an 8.8 × 10^{-2} M aqueous solution of **1**·NO3 at 1.8 K, measured at applied dc fields between zero and 10 kOe, with a 4 Oe oscillating ac field.

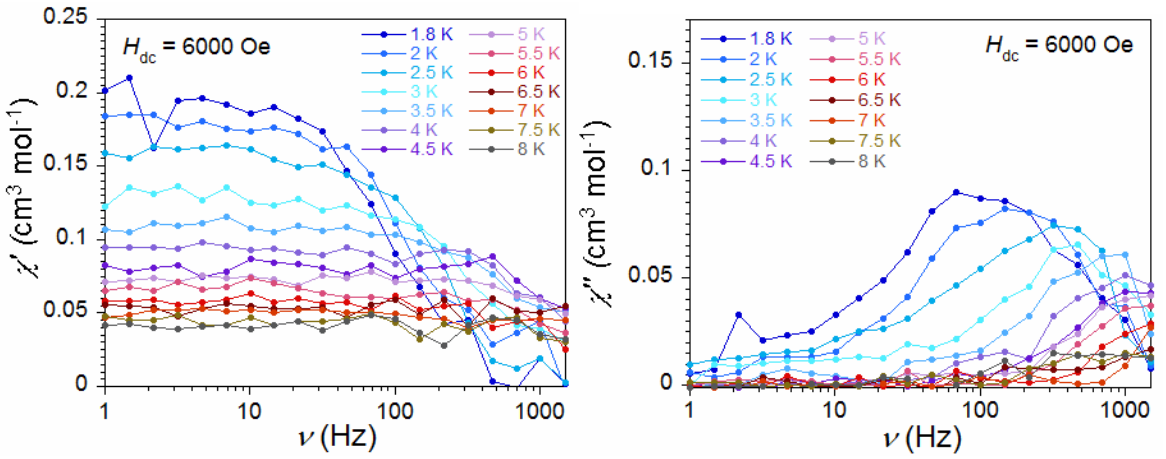

Figure S31. Frequency dependence of ac magnetic susceptibility for **1·NO$_3$(aq)**, measured at different temperatures at an applied dc field of 6000 Oe, with a 4 Oe oscillating ac field. In-phase (χ') ac magnetic susceptibility is shown at left; out-of-phase (χ'') ac magnetic susceptibility is shown at right.

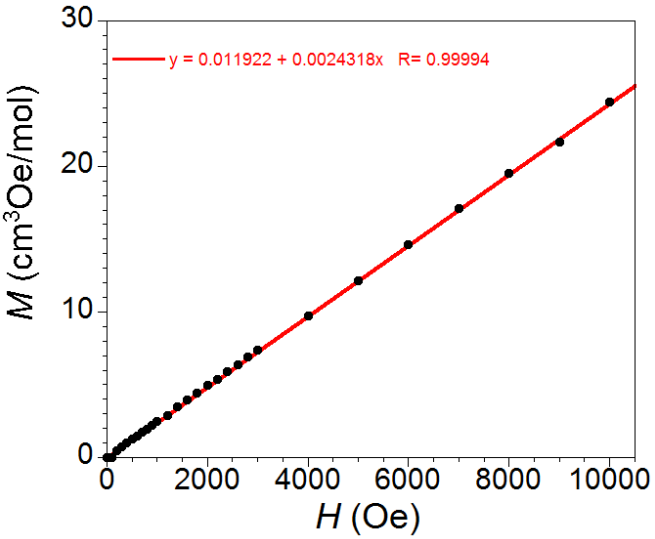

Figure S32. Plot of *M* vs. *H* for compound **3b**, collected at 100 K. The linear fit of the data (solid red line) indicates the absence of ferromagnetic impurities.

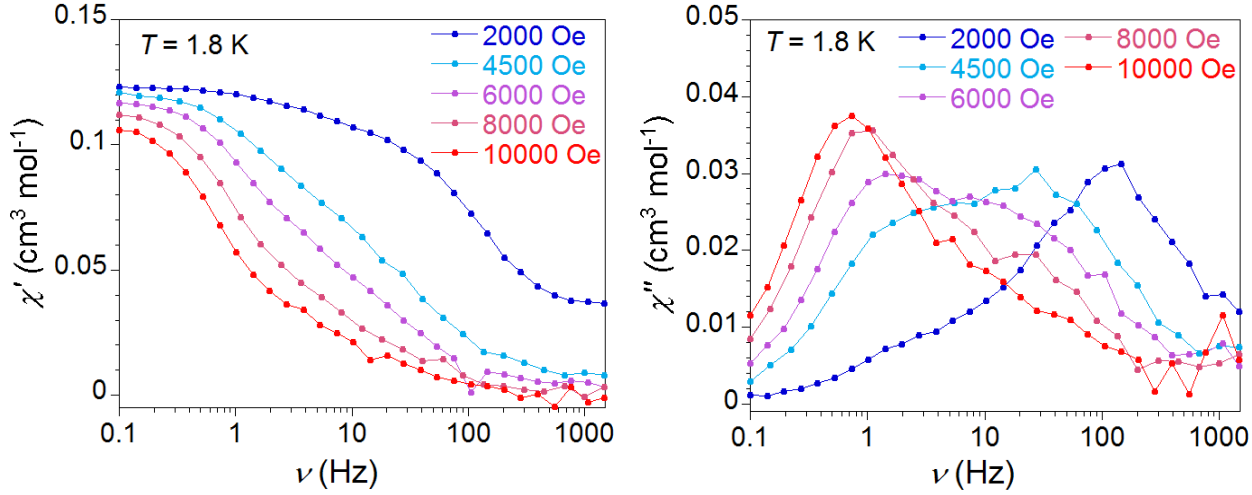

Figure S33. Frequency dependence of in-phase (χ') and out-of-phase (χ'') ac magnetic susceptibilities for **3b**, measured at 1.8 K at different applied dc fields between 2 kOe and 10 kOe, with a 4 Oe oscillating ac field.

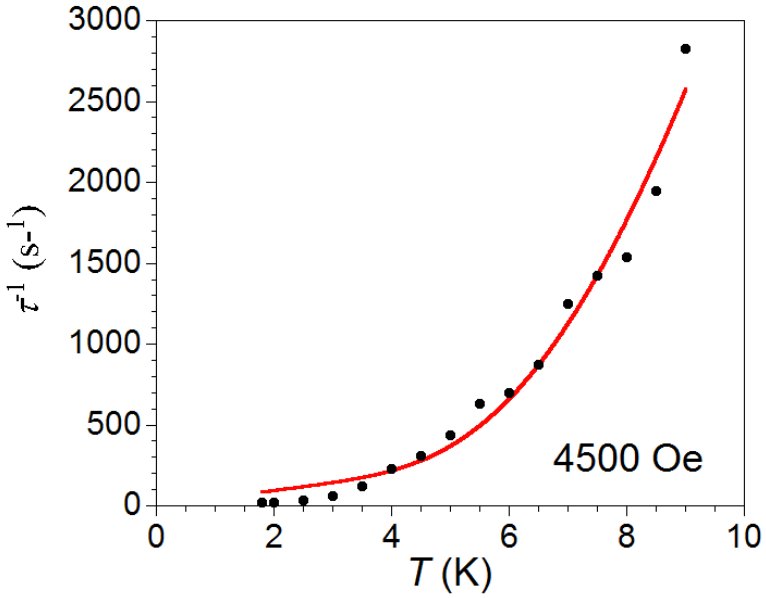

Figure S34. Attempt to fit τ^{-1} vs. T data for **1·NO$_3$** to a model combining direct and Orbach relaxation processes, using the equation $\tau^{-1} = AH^2T + \tau_0^{-1}\exp(-U_{eff}/T)$. The fit provides A = 0.12 s-1 kOe^{-2} K^{-1}, $U_{eff} \approx 31$ K and $\tau_0 = 1.43 \times 10^{-5}$ s. The goodness of fit (R = 0.988) is inferior to the direct + Raman model presented in the text.

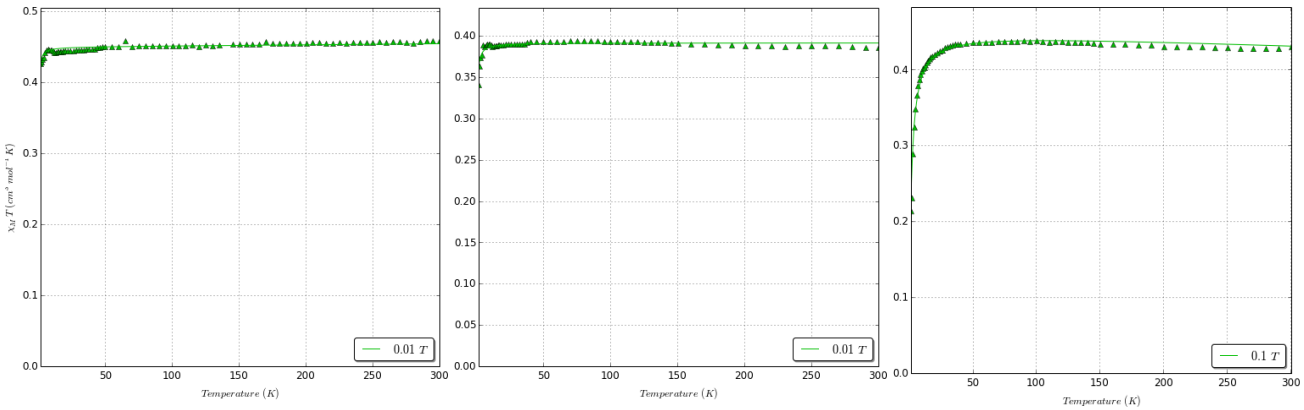

Figure S35. Fit of $\chi_M T$ vs T data for compound **1·NO$_3$**, **1·ClO$_4$** and **2·ClO$_4$** with the program PHI,[21] which extracts g_{iso} = 2.19(1), 2.04(2) and 2.19(2) respectively and respective mean field antiferromagetic interaction zJ/K = - 0.05(2), -0.09(1) and -0.91(1) K.

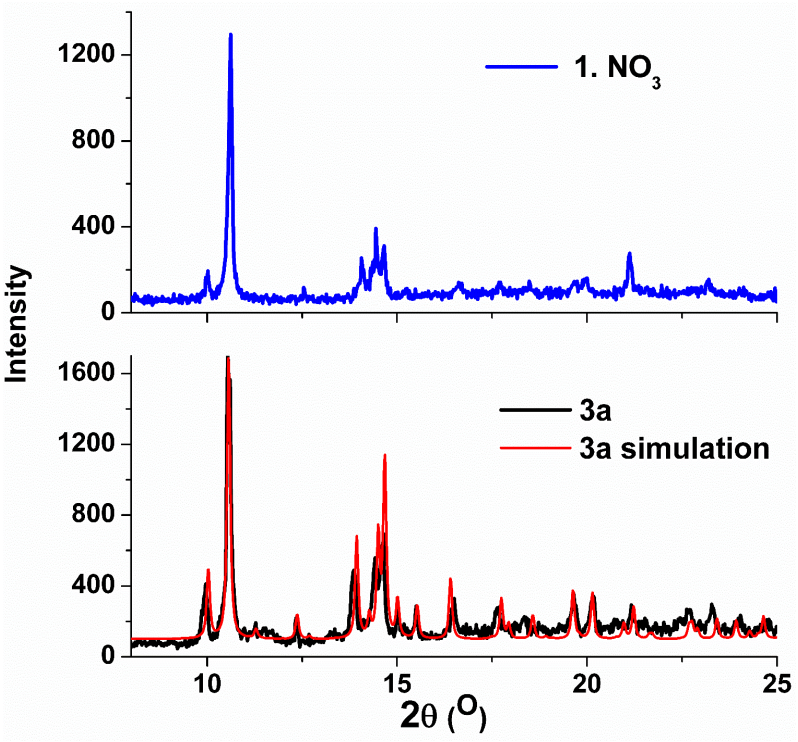

Figure S36. Powder X-ray diffraction (PXRD) data for **1·NO$_3$** (top) and **3a** (bottom), and comparison of **3a** to the simulation from single crystal X-ray diffraction data.

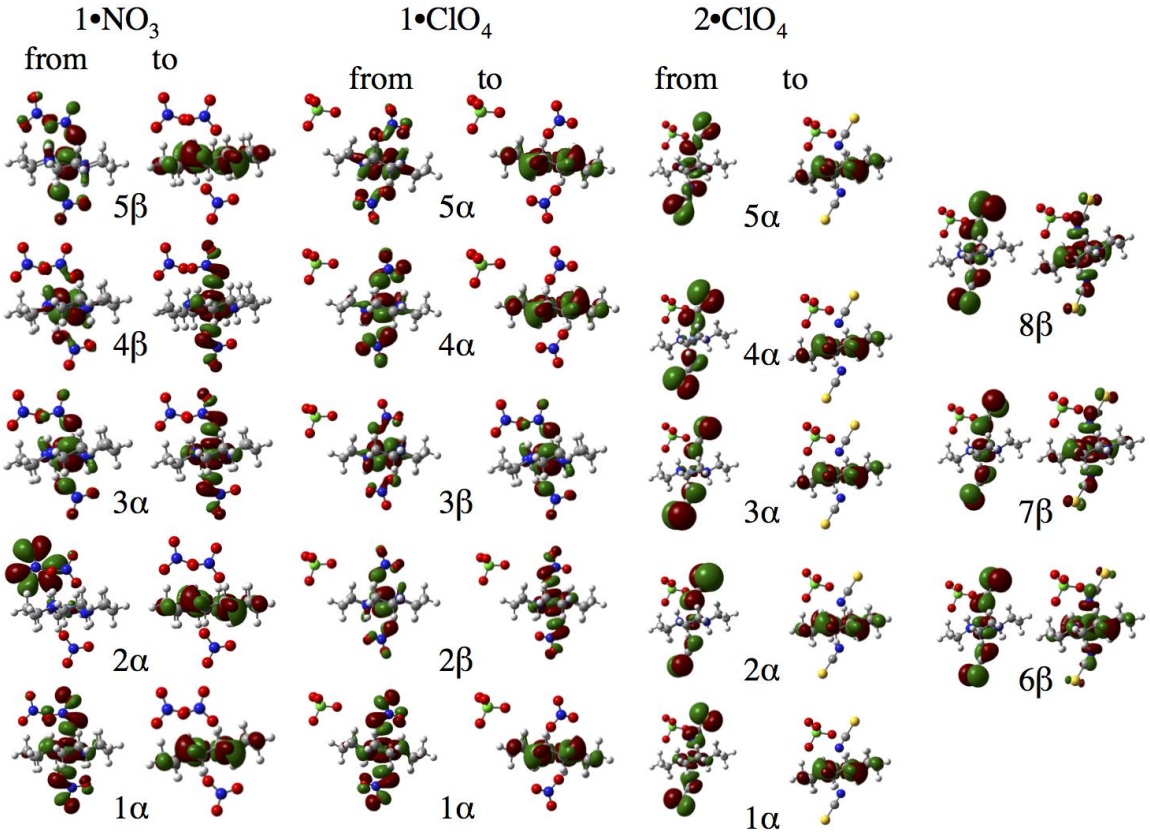

Figure S37. Natural transition orbitals (NTOs) for the low lying excied states of **1·NO$_3$, 1·ClO$_4$** and **2·ClO$_4$**.

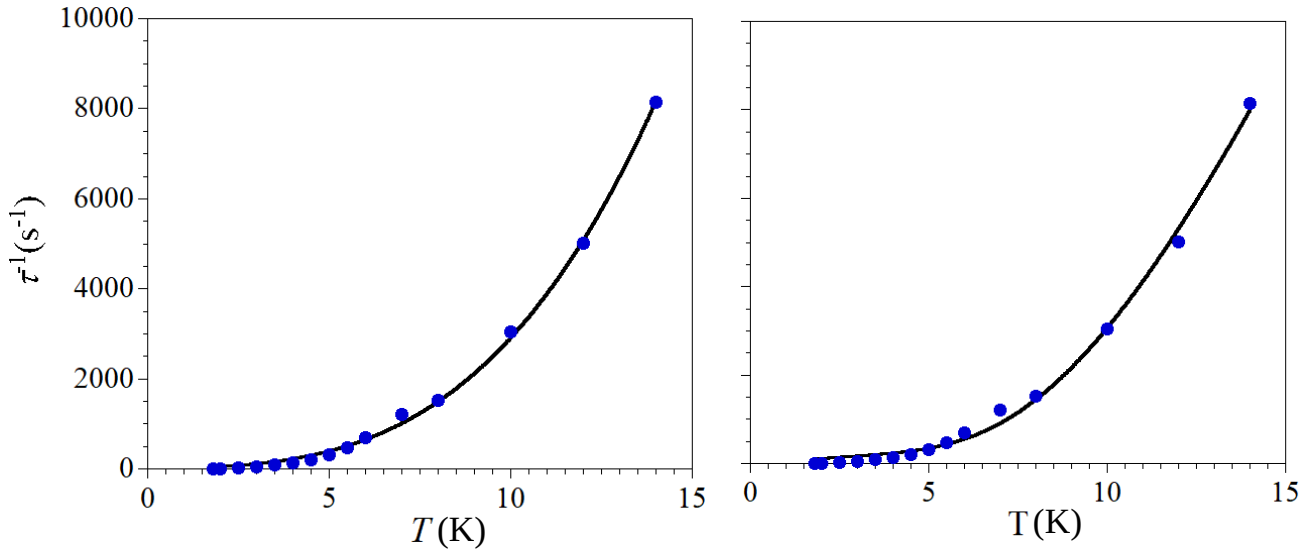

Figure S38. Temperature dependence of inverse magnetization lifetime for **1•ClO$_4$**. Left: the line represents the best fit (goodness of fit R = 0.999) for a combination of direct and Raman relaxation modes, with the equation $\tau^{-1} = AH^2T + BT^n$, which provided exponent n = 3.16(4), A = 0.93(4) and B = 1.87(4). Right: fit of the data combining direct and Orbach relaxation processes, using the equation $\tau^{-1} = AH^2T + \tau_0^{-1}\exp(-U_{eff}/T)$. The fit provides A = 2.83, $U_{eff} \approx 37$ K and $\tau_0 = 9.87 \times 10^{-6}$ s (goodness of fit R = 0.997).

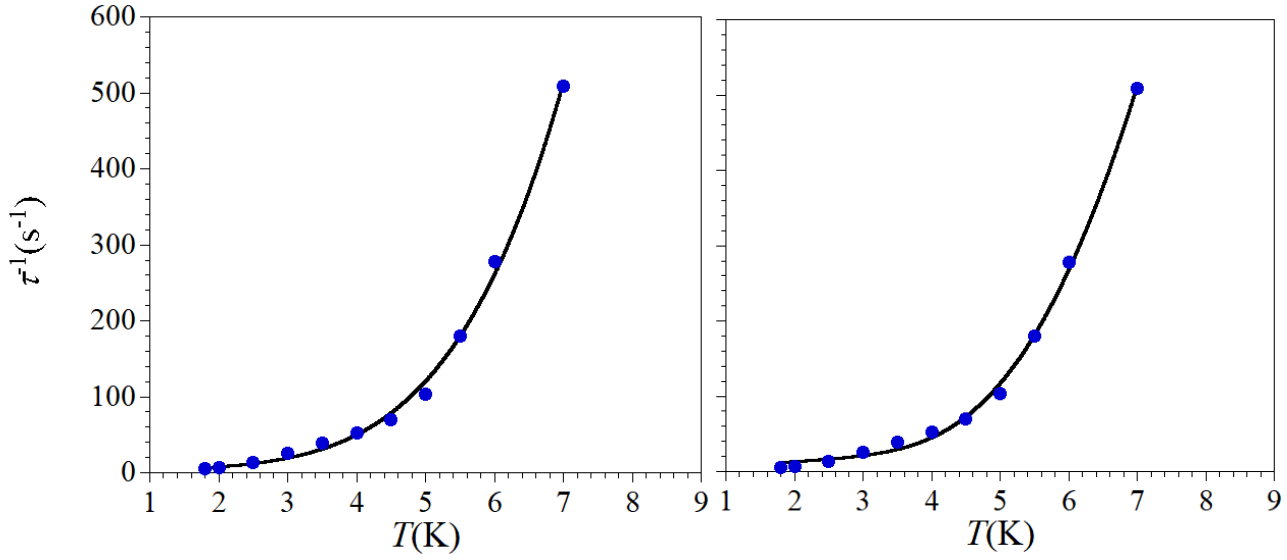

Figure S39. Temperature dependence of inverse magnetization lifetime for **3d**. (left) The line represents the best fit (goodness of fit R = 0.998) for a combination of Direct and Raman relaxation modes, with the equation $\tau^{-1} = AH^2T + BT^n$ which provided exponent n =4.59(1), A = 0.15(4) and B = 0.064(2). (right) fit of the data combining direct and Orbach relaxation processes, using the equation $\tau^{-1} = AH^2T + \tau_0^{-1}\exp(-U_{eff}/T)$. The fit provides A = 0.324(3), $U_{eff} \approx 30$ K and $\tau_0 = 2.96 \times 10^{-5}$ s. The goodness of fit (R = 0.998).

Table S4. TD-DFT calculated energies (cm^{-1}) of the excited states of **1·NO$_3$**, **1·ClO$_4$** and **2·ClO$_4$**

Excited state	**1·NO$_3$**	**1·ClO$_4$**	**2·ClO$_4$**
1	12386.18835	13501.647	7458.9744
2	14650.98075	15601.09665	10015.7379
3	15701.9154	16143.09825	11086.02975
4	16314.8934	19855.6479	11669.97195
5	19098.29745	20708.17125	13680.7011
6	19900.00815	21507.4623	14881.65405
7	20751.72495	21998.65125	15468.0159
8	21560.6946	22297.8813	16559.27805
9	21662.3199	23217.3483	17010.94605
10	22003.49055	23335.91115	17984.4519

Table S5. Coordinates for the computed structure for compound **1·NO$_3$**

atoms	x	y	z
Ni	6.408	0	0
O	4.487	0.169	0.899
O	4.33	2.356	0.952
O	2.757	1.116	1.796
N	7.257	1.019	1.466
N	6.653	-1.585	1.148
N	3.844	1.245	1.228
C	7.939	0.039	2.359
H	8.15259204	0.49040585	3.3278711
H	8.87685254	-0.2930416	1.91371245
C	6.995	-1.116	2.515
H	7.46728973	-1.9174614	3.08306876
H	6.09484356	-0.8008902	3.0427539
C	5.576	-2.606	1.191
H	4.67731806	-2.1643683	1.62161843
H	5.88643512	-3.4305245	1.83278609
C	7.556	3.14	0.194
H	8.23354684	3.98831068	0.09705021
H	6.6344254	3.50334483	0.64873155
C	8.184	2.115	1.115
H	9.06432767	1.69354313	0.62971937
H	8.5123616	2.61084805	2.0284623
H	6.46322022	1.42777282	2.01855628
H	7.49316584	-2.0552969	0.72914181
N	5.559	-1.019	-1.466
N	6.162	1.585	-1.148
C	4.877	-0.039	-2.359
H	4.66340796	-0.4904059	-3.3278711
H	3.93914746	0.29304158	-1.9137125
C	5.82	1.116	-2.515
H	5.34771027	1.91746135	-3.0830688

atoms	x	y	z
H	6.72015644	0.80089016	-3.0427539
C	7.24	2.606	-1.191
H	8.13868194	2.16436831	-1.6216184
H	6.92956488	3.4305245	-1.8327861
C	5.26	-3.14	-0.194
H	4.58177778	-3.9877778	-0.0971111
H	6.1815746	-3.5033448	-0.6487316
C	4.631	-2.115	-1.115
H	3.75105543	-1.6931993	-0.6293235
H	4.30364075	-2.6109989	-2.0287401
H	6.35226995	-1.4281227	-2.0190293
H	5.32183416	2.05529691	-0.7291418
O	8.328	-0.169	-0.899
O	8.486	-2.356	-0.952
O	0.059	-1.116	-1.796
N	8.972	-1.245	-1.228
O	4.314	3.535	4.126
O	5.3	1.654	3.665
N	5.3	2.929	3.665
O	6.285	3.535	3.204

Table S6. Coordinates for the computed structure for compound **1·ClO$_4$**

atoms	x	y	z
Ni	2.182	7.728	0
N	2.536	8.878	1.56
N	3.271	6.361	0.91
N	4.396	9.482	-1.26
O	4.013	8.329	-0.868
O	5.582	9.705	-1.396
O	3.544	10.316	-1.575
C	3.058	8.002	2.636
C	4.015	7.043	2.001
C	4.15	5.479	0.116
C	3.383	4.745	-0.955
C	1.472	9.782	2.042
H	3.30384107	9.54586176	1.30138686
H	2.50613735	5.78550849	1.34161863
H	3.55257224	8.64689466	3.36236711
H	2.13607539	7.5338512	2.98095175
H	4.31511674	6.29913088	2.73903027
H	4.91442028	7.46171581	1.54953546
H	4.58622221	4.92604227	0.94789418
H	4.95818923	6.13083367	-0.2157274
H	4.03751463	4.04346198	-1.4722572
H	2.56152446	4.16615896	-0.5328377

atoms	x	y	z
H	1.89641233	10.3200726	2.8896155
H	0.69358357	9.09955272	2.38322364
N	1.829	6.577	-1.56
N	1.094	9.094	-0.91
O	0.351	7.126	0.868
C	2.892	5.673	-2.042
C	0.982	10.71	0.955
C	1.307	7.453	-2.636
H	1.06053961	5.90975796	-1.3016268
C	0.349	8.412	-2.001
C	0.214	9.976	-0.116
H	1.85886265	9.66949151	-1.3416186
N	-0.032	5.973	1.26
H	2.46861417	5.13469516	-2.8899813
H	3.67099631	6.35491774	-2.3829589
H	0.32667356	11.4110469	1.47189508
H	1.80300496	11.2892767	0.53252
H	0.81151716	6.80841353	-3.36202
H	2.22892461	7.9211488	-2.9809518
H	0.04996298	9.15608821	-2.7392477
H	-0.55042028	7.99328419	-1.5495355
H	-0.22118952	10.529207	-0.9482692
H	-0.59418923	9.32416633	0.21572735
O	-1.218	5.75	1.396
O	0.82	5.139	1.575
C	-2.686	10.986	2.685
O	-1.892	12.082	2.243
O	-3.876	11.052	1.854
O	-3.057	11.147	4.027
O	-2.094	9.747	2.435

Table S7. Coordinates for the computed structure for compound **2·ClO_4**

atoms	x	y	z
Ni	5.705	4.972	7.757
S	9.491	7.763	7.199
N	4.993	6.841	7.707
H	3.95703729	6.74223682	7.56726061
N	5.624	5.111	9.75
H	6.59664072	5.34917631	10.0658197
C	8.46	6.513	7.581
N	7.691	5.655	7.845
C	5.456	7.807	6.63
H	4.88303687	8.73077933	6.71028082
H	6.50523372	8.05031653	6.79734893

atoms	x	y	z
C	5.296	7.252	5.262
H	5.51938918	8.03551279	4.53791093
H	4.25544459	6.95910292	5.12215816
C	5.156	7.41	9.08
H	4.51056866	8.27901933	9.20776457
H	6.18917238	7.7173082	9.24191508
C	5.21	3.915	10.549
H	4.17514478	3.66482733	10.3153586
H	5.26503046	4.15383221	11.611088
C	4.775	6.331	10.043
H	3.71886781	6.08541347	9.93177023
H	4.94436972	6.66753982	11.0658171
N	6.416	3.104	7.806
H	7.45182426	3.20274998	7.94677125
N	5.785	4.834	5.763
H	4.81258016	4.59482878	5.44725203
C	5.953	2.138	8.883
H	6.52596313	1.21422067	8.80271918
H	4.90376628	1.89468347	8.71565107
C	6.113	2.693	10.251
H	5.88961082	1.90948721	10.9750891
H	7.15355541	2.98589708	10.3908418
C	6.253	2.534	6.433
H	6.89843134	1.66498067	6.30523543
H	5.21953367	2.22770614	6.27103886
C	6.199	6.03	4.964
H	7.23363048	6.28011834	5.19869254
H	6.14396954	5.79116779	3.90191205
C	6.634	3.614	5.47
H	7.69013219	3.85958653	5.58122977
H	6.46446978	3.27714126	4.44731447
S	1.918	2.182	8.314
C	2.949	3.431	7.932
N	3.718	4.29	7.668
Cl	8.48037173	7.16879263	11.7991838
O	9.27150686	7.66206795	12.9746753
O	7.39684321	6.2474361	12.276744
O	9.38770303	6.42955404	10.860423
O	7.86543382	8.33611241	11.0848929

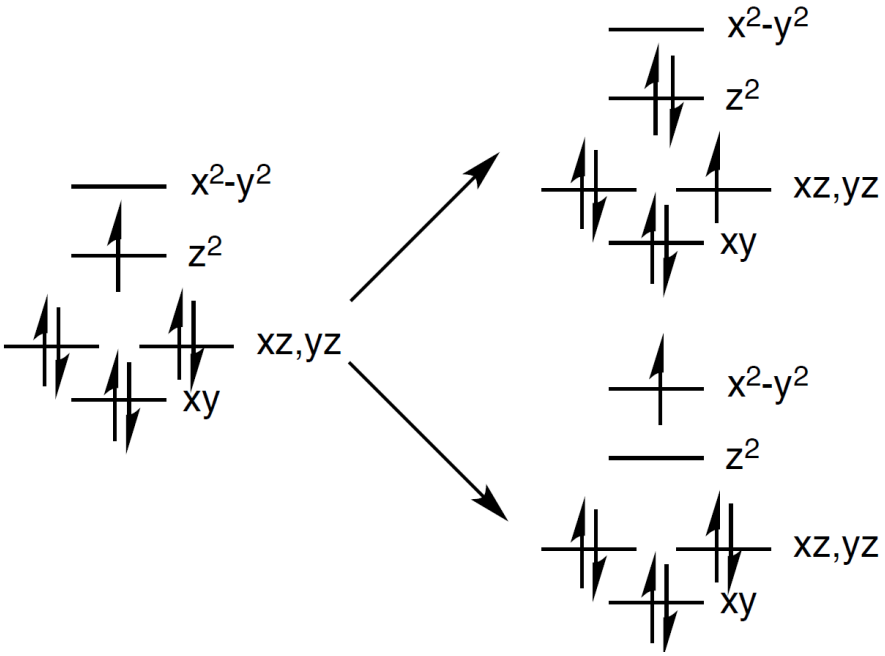

Figure S40. Orbitals involved in low-energy electronic (d-d) transitions relevant to interpretation of diffuse reflectance spectra for the Ni(III) cyclam complexes.

Note that promotion of an electron from the d_{xz}/d_{yz} set (top) generates the possibility for unquenched orbital angular momentum, while promotion from the axial d_{z2} orbtial (bottom) does not lead to orbital contributions.

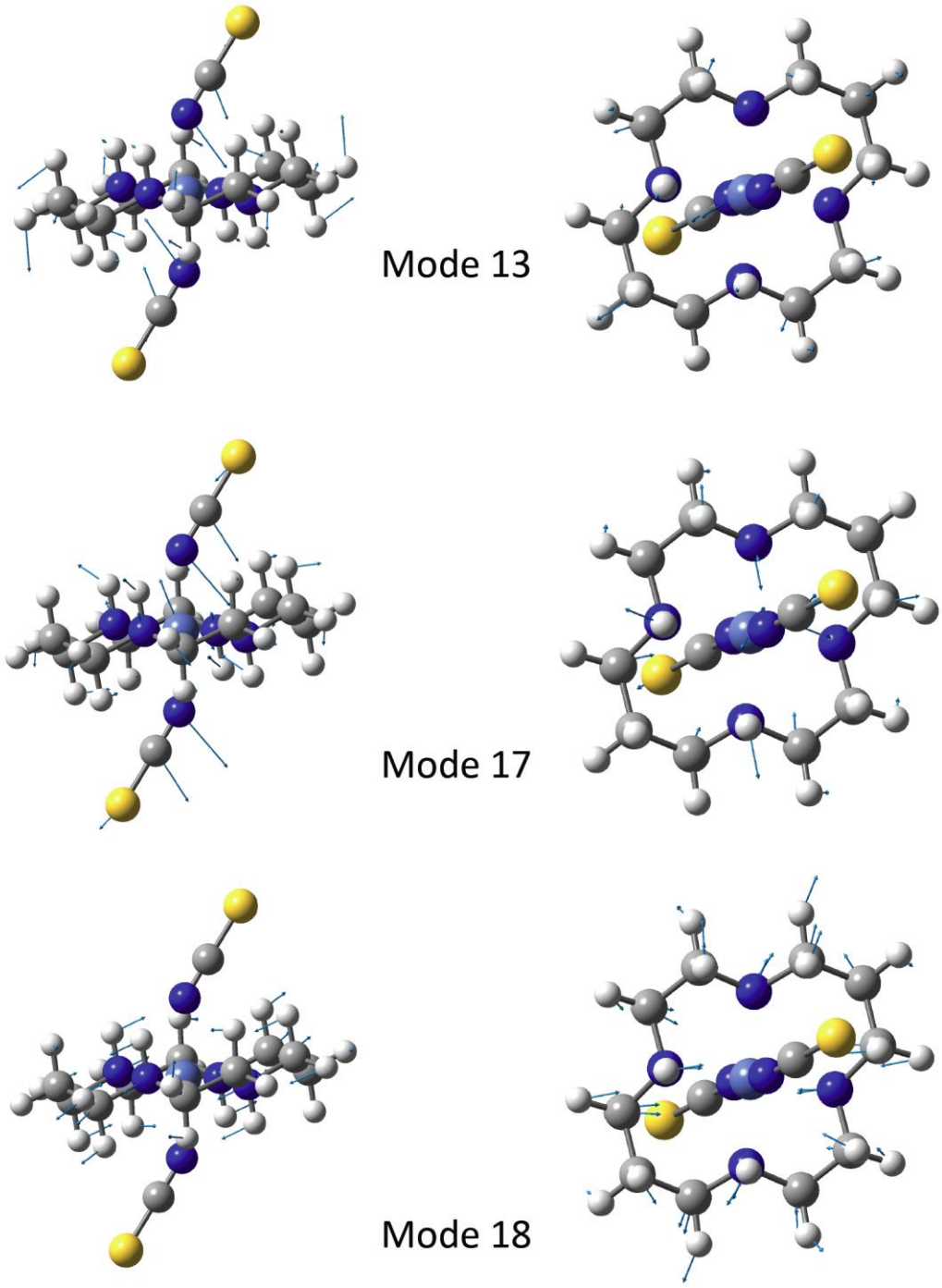

Figure S41. Key (computed) vibrational modes for **2·ClO$_4$** contributing to observed *g* and/or *A* anisotropy.

Table S8. Computed *g* values (B3LYP, ESR2 basis in ORCA) for **1·NO$_3$** and **2·ClO$_4$**

Complex	g_{zz}	g_{xx}	g_{yy}	g_{iso}
1·NO$_3$	2.032	2.151	2.157	2.113
2·ClO$_4$	2.034	2.132	2.136	2.101

Table S9. Computed Nitrogen *A* values (B3LYP, ESR2 basis in ORCA) for **1·NO$_3$** and **2·ClO$_4$**

Complex	Nitrogen	A_{Nzz} [a]	A_{Nxx} [a]	A_{Nyy} [a]	A_{Niso} [a]
1·NO$_3$	1	1.69	2.28	2.96	2.31
	2	0.24	1.18	1.55	0.99
	3[b]	0.11	0.38	1.57	0.68
	4	1.66	2.27	2.94	2.29
	5	0.24	1.18	1.56	1.00
	6[b]	0.12	0.39	1.58	0.70
2·ClO$_4$	1	4.24	4.90	5.81	4.98
	2	4.37	4.97	5.92	5.09
	3[c]	54.14	55.10	62.09	57.1
	4	4.26	4.91	5.82	5.00
	5	4.36	4.97	5.91	5.08
	6[c]	54.15	55.11	62.10	57.12

[a] *A* values given in MHz; [b] these sites are oxygen atoms from nitrato ligands; [c] N atoms from NCS^- ligands.

Table S10. Computed variation in *g* for significant vibrational modes in **2·ClO$_4$** (modes where the magnitude of the 1st/2nd derivative is greater than 0.01)

displacement	mode	g_{zz}	g_{xx}	g_{yy}	g_{iso}	Δg_{zz}	Δg_{xx}	Δg_{yy}	Δg_{iso}
-	7	2.035	2.14	2.145	2.107	0	-0.008	-0.009	-0.006
+		2.034	2.126	2.129	2.097	0	0.006	0.007	0.004
1st deriv.						0	0.007	0.008	
-	13	2.033	2.156	2.159	2.116	0.001	-0.024	-0.023	-0.015
+		2.035	2.108	2.113	2.085	0	0.024	0.023	0.016
1st deriv.						-0.001	0.024	0.023	
-	14	2.035	2.137	2.139	2.104	0	-0.004	-0.003	-0.003
+		2.035	2.126	2.135	2.099	0	0.006	0.001	0.002
1st deriv.						0	0.005	0.002	
-	15	2.038	2.128	2.136	2.101	-0.003	0.004	0	0
+		2.032	2.129	2.144	2.102	0.003	0.003	-0.008	-0.001
1st deriv.						0.003	-0.001	-0.004	
-	17	2.034	2.125	2.128	2.096	0	0.008	0.008	0.005
+		2.034	2.125	2.128	2.096	0	0.008	0.008	0.005
2nd deriv.						0	0.008	0.008	
-	18	2.036	2.106	2.158	2.1	-0.001	0.026	-0.022	0.001
+		2.035	2.107	2.158	2.1	-0.001	0.025	-0.022	0.001
2nd deriv.						-0.001	0.026	-0.022	

Table S11. Computed variation in *A* for significant vibrational modes in **2·ClO$_4$** (modes where the magnitude of the 1st/2nd derivative is greater than 1.0). Nitrogen atoms 3 & 6 correspond to axial isothiocyanato ligands.

displacement, mode, N atom	A_{xx}	A_{yy}	A_{zz}	A_{iso}	ΔA_{xx}	ΔA_{yy}	ΔA_{zz}	ΔA_{iso}
- 2 6	54.4	55.3	62.2	57.3	0.2	0.2	0.1	0.2
+	53.7	54.7	61.6	56.7	-0.4	-0.4	-0.5	-0.4
1st deriv.					-0.3	-0.3	-0.3	
- 3 3	56.5	57.2	64.2	59.3	2.3	2.1	2.1	2.2
+	51.9	53	59.9	54.9	-2.3	-2.1	-2.2	-2.2
1st deriv.					-2.3	-2.1	-2.2	
- 3 6	51.9	53	59.9	54.9	-2.3	-2.1	-2.2	-2.2
+	56.5	57.2	64.2	59.3	2.3	2.1	2.1	2.2
1st deriv.					2.3	2.1	2.2	
- 4 3	50.4	51.5	58.4	53.4	-3.7	-3.6	-3.7	-3.7
+	57.4	58.1	65.1	60.2	3.2	3	3	3.1
1st deriv.					3.5	3.3	3.4	
- 4 6	50.4	51.5	58.4	53.4	-3.8	-3.6	-3.7	-3.7
+	57.4	58.1	65	60.2	3.2	3	2.9	3
1st deriv.					3.5	3.3	3.3	
- 5 3	53.6	54.6	61.5	56.5	-0.6	-0.5	-0.6	-0.6
+	54.8	55.7	62.7	57.8	0.7	0.6	0.6	0.6
1st deriv.					0.6	0.6	0.6	
- 5 6	54.7	55.7	62.7	57.7	0.6	0.5	0.6	0.6
+	53.5	54.5	61.5	56.5	-0.6	-0.6	-0.6	-0.6
1st deriv.					-0.6	-0.6	-0.6	
- 6 1	5	5.7	6.8	5.8	0.8	0.8	0.9	0.8
+	3.4	4.1	4.8	4.1	-0.9	-0.8	-1	-0.9
1st deriv.					-0.9	-0.8	-0.9	
- 6 2	3.8	4.5	5.3	4.5	-0.5	-0.5	-0.6	-0.6
+	4.9	5.5	6.6	5.7	0.5	0.5	0.7	0.6
1st deriv.					0.5	0.5	0.6	
- 6 4	3.4	4.1	4.8	4.1	-0.9	-0.8	-1.1	-0.9
+	5	5.7	6.8	5.8	0.8	0.8	1	0.8
1st deriv.					0.9	0.8	1.1	
- 6 5	4.9	5.5	6.6	5.6	0.5	0.5	0.6	0.6
+	3.8	4.4	5.3	4.5	-0.6	-0.5	-0.6	-0.6
1st deriv.					-0.6	-0.5	-0.6	
- 7 1	3.4	4.5	5.2	4.2	-0.8	-0.4	-0.6	-0.8
+	4.8	5.5	6.5	5.6	0.5	0.6	0.7	0.6
1st deriv.					0.7	0.5	0.6	
- 7 2	3.6	4.2	5	4.3	-0.8	-0.7	-0.9	-0.8
+	5	5.6	6.7	5.8	0.7	0.7	0.8	0.7
1st deriv.					0.8	0.7	0.9	
- 7 3	56.3	57	63.9	59.1	2.2	1.9	1.8	2
+	50.9	52.1	59.1	54	-3.3	-3	-3	-3.1

displacement, mode, N atom	A_{xx}	A_{yy}	A_{zz}	A_{iso}	ΔA_{xx}	ΔA_{yy}	ΔA_{zz}	ΔA_{iso}
1st deriv.					-2.8	-2.5	-2.4	
- 7 4	3.5	4.2	4.9	4.2	-0.8	-0.7	-0.9	-0.8
+	4.8	5.5	6.5	5.6	0.5	0.6	0.7	0.6
1st deriv.					0.7	0.6	0.8	
- 7 5	3.6	4.2	5	4.3	-0.8	-0.7	-0.9	-0.8
+	5	5.6	6.7	5.8	0.7	0.7	0.8	0.7
1st deriv.					0.8	0.7	0.9	
- 7 6	56.3	57	63.9	59.1	2.2	1.9	1.8	1.9
+	50.9	52.2	59.1	54.1	-3.3	-3	-3	-3.1
1st deriv.					-2.8	-2.5	-2.4	
- 8 1	4.7	5.3	6.4	5.4	0.4	0.4	0.5	0.5
+	3.9	4.6	5.3	4.6	-0.3	-0.3	-0.5	-0.4
1st deriv.					-0.3	-0.3	-0.5	
- 8 2	4.9	5.5	6.6	5.7	0.6	0.6	0.7	0.6
+	3.8	4.4	5.2	4.5	-0.6	-0.5	-0.7	-0.6
1st deriv.					-0.6	-0.6	-0.7	
- 8 3	53.7	54.6	61.6	56.6	-0.5	-0.5	-0.5	-0.5
+	54.4	55.4	62.4	57.4	0.3	0.3	0.3	0.3
1st deriv.					0.4	0.4	0.4	
- 8 4	3.9	4.5	5.3	4.6	-0.4	-0.4	-0.5	-0.4
+	4.7	5.3	6.4	5.5	0.4	0.4	0.6	0.5
1st deriv.					0.4	0.4	0.6	
- 8 5	3.7	4.4	5.2	4.4	-0.6	-0.6	-0.8	-0.7
+	5	5.6	6.7	5.8	0.6	0.6	0.8	0.7
1st deriv.					0.6	0.6	0.8	
- 9 1	4.7	5.2	6.3	5.4	0.4	0.3	0.5	0.4
+	3.7	4.4	5.2	4.4	-0.6	-0.5	-0.6	-0.6
1st deriv.					-0.5	-0.4	-0.6	
- 9 2	3.8	4.6	5.4	4.6	-0.5	-0.4	-0.5	-0.5
+	4.7	5.2	6.3	5.4	0.3	0.3	0.4	0.3
1st deriv.					0.4	0.3	0.5	
- 9 3	53.3	54.3	61.3	56.3	-0.9	-0.8	-0.8	-0.8
+	54.1	55.1	62	57	-0.1	-0.1	-0.1	-0.1
1st deriv.					0.4	0.4	0.4	
- 9 4	4.8	5.4	6.4	5.5	0.6	0.5	0.6	0.6
+	3.5	4.3	5	4.3	-0.8	-0.6	-0.8	-0.7
1st deriv.					-0.7	-0.6	-0.7	
- 9 5	3.8	4.5	5.4	4.6	-0.5	-0.4	-0.6	-0.5
+	4.8	5.3	6.4	5.5	0.4	0.3	0.5	0.4
1st deriv.					0.5	0.3	0.6	
- 10 1	1.9	3	3.6	2.8	-2.3	-1.9	-2.3	-2.2
+	6.1	6.5	7.8	6.8	1.8	1.6	2	1.8

displacement, mode, N atom	A_{xx}	A_{yy}	A_{zz}	A_{iso}	ΔA_{xx}	ΔA_{yy}	ΔA_{zz}	ΔA_{iso}
1st deriv.					2	1.8	2.1	
- 10 2	5.7	6.1	7.3	6.4	1.3	1.1	1.4	1.3
+	2.8	3.7	4.4	3.7	-1.6	-1.3	-1.5	-1.4
1st deriv.					-1.5	-1.2	-1.4	
- 10 3	49.3	50.6	57.6	52.5	-4.9	-4.5	-4.4	-4.6
+	57	57.6	64.4	59.7	2.9	2.5	2.3	2.5
2nd deriv.					-1	-1	-1.1	
- 10 3	49.3	50.6	57.6	52.5	-4.9	-4.5	-4.4	-4.6
+	57	57.6	64.4	59.7	2.9	2.5	2.3	2.5
1st deriv.					3.9	3.5	3.4	
- 10 4	6.1	6.5	7.8	6.8	1.8	1.6	2	1.8
+	1.9	3	3.6	2.8	-2.3	-1.9	-2.3	-2.2
1st deriv.					-2	-1.8	-2.1	
- 10 5	2.8	3.7	4.4	3.7	-1.5	-1.2	-1.5	-1.4
+	5.7	6.1	7.4	6.4	1.4	1.1	1.4	1.3
1st deriv.					1.4	1.1	1.4	
- 10 6	57	57.5	64.3	59.6	2.8	2.4	2.2	2.5
+	49.2	50.5	57.6	52.5	-4.9	-4.6	-4.5	-4.7
2nd deriv.					-1.1	-1.1	-1.1	
- 10 6	57	57.5	64.3	59.6	2.8	2.4	2.2	2.5
+	49.2	50.5	57.6	52.5	-4.9	-4.6	-4.5	-4.7
1st deriv.					-3.9	-3.5	-3.4	
- 11 1	5.8	6.5	7.8	6.7	1.6	1.6	2	1.7
+	2.1	2.8	3.3	2.7	-2.2	-2.1	-2.5	-2.2
1st deriv.					-1.9	-1.9	-2.2	
- 11 2	6.6	7.1	8.7	7.5	2.3	2.2	2.7	2.4
+	1.4	2.3	2.7	2.1	-3	-2.7	-3.2	-3
1st deriv.					-2.6	-2.5	-3	
- 11 3	51.5	52.6	59.5	54.5	-2.7	-2.6	-2.6	-2.6
+	51.7	52.7	59.7	54.7	-2.5	-2.4	-2.4	-2.4
2nd deriv.					-2.6	-2.5	-2.5	
- 11 4	2.1	2.8	3.3	2.7	-2.2	-2.1	-2.5	-2.3
+	5.8	6.5	7.8	6.7	1.6	1.6	1.9	1.7
1st deriv.					1.9	1.9	2.2	
- 11 5	1.4	2.3	2.7	2.1	-3	-2.7	-3.2	-3
+	6.6	7.1	8.7	7.5	2.3	2.2	2.7	2.4
1st deriv.					2.6	2.5	3	
- 11 6	51.7	52.7	59.7	54.7	-2.5	-2.4	-2.5	-2.4
+	51.5	52.5	59.5	54.5	-2.7	-2.6	-2.7	-2.6
2nd deriv.					-2.6	-2.5	-2.6	
- 12 1	5.4	5.9	7.2	6.2	1.2	1	1.4	1.2
+	3.1	3.9	4.5	3.8	-1.2	-1	-1.3	-1.2

displacement, mode, N atom	A_{xx}	A_{yy}	A_{zz}	A_{iso}	ΔA_{xx}	ΔA_{yy}	ΔA_{zz}	ΔA_{iso}
1st deriv.					-1.2	-1	-1.4	
- 12 2	3.4	4.1	4.8	4.1	-1	-0.8	-1.2	-1
+	5.3	5.8	7.1	6.1	0.9	0.9	1.2	1
1st deriv.					0.9	0.9	1.2	
- 12 4	5.4	6	7.2	6.2	1.2	1	1.4	1.2
+	3.1	3.9	4.5	3.8	-1.2	-1	-1.3	-1.2
1st deriv.					-1.2	-1	-1.4	
- 12 5	3.3	4.1	4.7	4.1	-1	-0.9	-1.2	-1
+	5.3	5.8	7.1	6.1	0.9	0.9	1.2	1
1st deriv.					0.9	0.9	1.2	
- 13 1	1.5	2.4	3	2.3	-2.7	-2.5	-2.8	-2.7
+	7.7	8.2	9.5	8.5	3.5	3.3	3.7	3.5
1st deriv.					3.1	2.9	3.2	
- 13 2	1.4	2.3	2.8	2.2	-2.9	-2.7	-3.1	-2.9
+	8.9	9.3	11.1	9.8	4.6	4.3	5.2	4.7
2nd deriv.					0.8	0.8	1.1	
- 13 2	1.4	2.3	2.8	2.2	-2.9	-2.7	-3.1	-2.9
+	8.9	9.3	11.1	9.8	4.6	4.3	5.2	4.7
1st deriv.					3.8	3.5	4.2	
- 13 3	43.8	44.8	51.7	46.8	-10.4	-10.3	-10.4	-10.3
+	62.6	63.4	70.5	65.5	8.5	8.3	8.4	8.4
2nd deriv.					-1	-1	-1	
- 13 3	43.8	44.8	51.7	46.8	-10.4	-10.3	-10.4	-10.3
+	62.6	63.4	70.5	65.5	8.5	8.3	8.4	8.4
1st deriv.					9.4	9.3	9.4	
- 13 4	1.5	2.4	3	2.3	-2.7	-2.5	-2.8	-2.7
+	7.8	8.2	9.6	8.5	3.5	3.3	3.7	3.5
1st deriv.					3.1	2.9	3.2	
- 13 5	1.4	2.2	2.8	2.2	-2.9	-2.7	-3.1	-2.9
+	8.9	9.3	11.1	9.8	4.6	4.3	5.2	4.7
2nd deriv.					0.8	0.8	1.1	
- 13 5	1.4	2.2	2.8	2.2	-2.9	-2.7	-3.1	-2.9
+	8.9	9.3	11.1	9.8	4.6	4.3	5.2	4.7
1st deriv.					3.8	3.5	4.2	
- 13 6	43.8	44.8	51.8	46.8	-10.4	-10.3	-10.3	-10.3
+	62.6	63.4	70.4	65.5	8.5	8.3	8.3	8.3
2nd deriv.					-1	-1	-1	
- 13 6	43.8	44.8	51.8	46.8	-10.4	-10.3	-10.3	-10.3
+	62.6	63.4	70.4	65.5	8.5	8.3	8.3	8.3
1st deriv.					9.4	9.3	9.3	
- 14 2	3.7	4.3	5.1	4.4	-0.6	-0.6	-0.8	-0.7
+	5.1	5.7	6.9	5.9	0.8	0.7	0.9	0.8

displacement, mode, N atom	A_{xx}	A_{yy}	A_{zz}	A_{iso}	ΔA_{xx}	ΔA_{yy}	ΔA_{zz}	ΔA_{iso}
1st deriv.					0.7	0.6	0.9	
- 14 3	52.2	53.2	60.2	55.2	-1.9	-1.9	-1.9	-1.9
+	55.8	56.7	63.7	58.8	1.7	1.6	1.6	1.7
1st deriv.					1.8	1.8	1.8	
- 14 5	3.7	4.3	5.1	4.4	-0.7	-0.6	-0.8	-0.7
+	5.1	5.7	6.8	5.9	0.7	0.7	0.9	0.8
1st deriv.					0.7	0.6	0.9	
- 14 6	52.2	53.2	60.2	55.2	-1.9	-1.9	-1.9	-1.9
+	55.9	56.8	63.8	58.8	1.7	1.7	1.7	1.7
1st deriv.					1.8	1.8	1.8	
- 15 1	3.7	4.5	5.2	4.5	-0.5	-0.4	-0.6	-0.5
+	4.4	5	6.1	5.2	0.2	0.1	0.3	0.2
1st deriv.					0.3	0.2	0.4	
- 15 2	5.7	6.1	7.3	6.4	1.3	1.2	1.4	1.3
+	3.2	4	4.8	4	-1.2	-1	-1.1	-1.1
1st deriv.					-1.2	-1.1	-1.2	
- 15 3	56	56.8	63.8	58.9	1.9	1.7	1.7	1.8
+	51.5	52.6	59.6	54.6	-2.6	-2.5	-2.5	-2.5
1st deriv.					-2.2	-2.1	-2.1	
- 15 4	3.7	4.6	5.2	4.5	-0.5	-0.4	-0.6	-0.5
+	4.4	5	6.1	5.2	0.1	0.1	0.3	0.2
1st deriv.					0.3	0.2	0.4	
- 15 5	5.7	6.1	7.3	6.4	1.3	1.2	1.4	1.3
+	3.2	4	4.8	4	-1.2	-1	-1.1	-1.1
1st deriv.					-1.2	-1.1	-1.2	
- 15 6	56.1	56.9	63.8	58.9	1.9	1.8	1.7	1.8
+	51.5	52.6	59.6	54.6	-2.6	-2.5	-2.5	-2.5
1st deriv.					-2.2	-2.1	-2.1	
- 16 1	4.6	5.1	6.1	5.3	0.3	0.2	0.3	0.3
+	3.9	4.6	5.5	4.7	-0.4	-0.3	-0.3	-0.3
1st deriv.					-0.3	-0.2	-0.3	
- 16 3	54.7	55.7	62.7	57.7	0.6	0.6	0.6	0.6
+	53.5	54.5	61.4	56.5	-0.6	-0.6	-0.7	-0.6
1st deriv.					-0.6	-0.6	-0.6	
- 16 4	3.9	4.6	5.5	4.7	-0.4	-0.3	-0.3	-0.3
+	4.6	5.2	6.1	5.3	0.3	0.2	0.3	0.3
1st deriv.					0.3	0.2	0.3	
- 16 6	53.5	54.5	61.5	56.5	-0.6	-0.6	-0.6	-0.6
+	54.7	55.7	62.7	57.7	0.6	0.5	0.6	0.6
1st deriv.					0.6	0.6	0.6	
- 17 1	5.6	6.1	7	6.2	1.3	1.2	1.2	1.2
+	3.5	4.2	5.3	4.3	-0.8	-0.7	-0.5	-0.7

displacement, mode, N atom	A_{xx}	A_{yy}	A_{zz}	A_{iso}	ΔA_{xx}	ΔA_{yy}	ΔA_{zz}	ΔA_{iso}
1st deriv.					-1.1	-0.9	-0.8	
- 17 2	3.8	4.5	5.7	4.7	-0.5	-0.5	-0.3	-0.4
+	5.6	6	7	6.2	1.2	1	1	1.1
1st deriv.					0.8	0.8	0.7	
- 17 3	73.6	74.4	83.3	77.1	19.4	19.3	21.2	20
+	34.2	35.1	39.9	36.4	-19.9	-20	-22.2	-20.7
1st deriv.					-19.6	-19.6	-21.7	
- 17 4	3.4	4.2	5.2	4.3	-0.8	-0.7	-0.6	-0.7
+	5.6	6.1	7.1	6.3	1.4	1.2	1.3	1.3
1st deriv.					1.1	0.9	0.9	
- 17 5	5.6	6	7	6.2	1.2	1.1	1.1	1.1
+	3.8	4.5	5.6	4.6	-0.6	-0.5	-0.3	-0.5
1st deriv.					-0.9	-0.8	-0.7	
- 17 6	34.2	35.1	39.9	36.4	-19.9	-20	-22.2	-20.7
+	73.6	74.4	83.3	77.1	19.4	19.2	21.2	19.9
1st deriv.					19.6	19.6	21.7	
- 18 1	11.7	11.9	16.4	13.4	7.5	7	10.6	8.4
+	0.2	0.5	-1.9	-0.4	-4	-4.4	-7.7	-5.4
2nd deriv.					1.8	1.3	1.4	
- 18 1	11.7	11.9	16.4	13.4	7.5	7	10.6	8.4
+	0.2	0.5	-1.9	-0.4	-4	-4.4	-7.7	-5.4
1st deriv.					-5.8	-5.7	-9.2	
- 18 2	0.2	0.5	-1.9	-0.4	-4.2	-4.5	-7.8	-5.5
+	11.5	11.6	16.1	13.1	7.1	6.7	10.2	8
2nd deriv.					1.4	1.1	1.2	
- 18 2	0.2	0.5	-1.9	-0.4	-4.2	-4.5	-7.8	-5.5
+	11.5	11.6	16.1	13.1	7.1	6.7	10.2	8
1st deriv.					5.7	5.6	9	
- 18 3	51	51.9	58.4	53.8	-3.2	-3.2	-3.6	-3.3
+	50.5	51.4	58	53.3	-3.7	-3.7	-4.1	-3.8
2nd deriv.					-3.5	-3.5	-3.8	
- 18 4	11.7	11.9	16.4	13.4	7.5	7	10.6	8.4
+	0.2	0.5	-1.9	-0.4	-4	-4.4	-7.7	-5.4
2nd deriv.					1.8	1.3	1.4	
- 18 4	11.7	11.9	16.4	13.4	7.5	7	10.6	8.4
+	0.2	0.5	-1.9	-0.4	-4	-4.4	-7.7	-5.4
1st deriv.					-5.8	-5.7	-9.2	
- 18 5	0.2	0.5	-1.9	-0.4	-4.2	-4.5	-7.8	-5.5
+	11.5	11.6	16.1	13.1	7.1	6.7	10.2	8
2nd deriv.					1.4	1.1	1.2	
- 18 5	0.2	0.5	-1.9	-0.4	-4.2	-4.5	-7.8	-5.5
+	11.5	11.6	16.1	13.1	7.1	6.7	10.2	8

displacement, mode, N atom	A_{xx}	A_{yy}	A_{zz}	A_{iso}	ΔA_{xx}	ΔA_{yy}	ΔA_{zz}	ΔA_{iso}
1st deriv.					5.7	5.6	9	
- 18 6	51	51.9	58.5	53.8	-3.1	-3.2	-3.6	-3.3
+	50.5	51.4	58	53.3	-3.7	-3.7	-4.1	-3.8
2nd deriv.					-3.4	-3.5	-3.8	
- 19 1	4.9	5.2	6.3	5.5	0.6	0.3	0.5	0.5
+	3.2	4.3	5.1	4.2	-1.1	-0.6	-0.7	-0.8
1st deriv.					-0.9	-0.4	-0.6	
- 19 2	3.2	4.4	5.1	4.2	-1.2	-0.6	-0.8	-0.9
+	5	5.3	6.5	5.6	0.6	0.3	0.6	0.5
1st deriv.					0.9	0.4	0.7	
- 19 3	54.3	55.5	62.8	57.5	0.1	0.4	0.7	0.4
+	52.6	53.4	59.9	55.3	-1.5	-1.7	-2.2	-1.8
2nd deriv.					-0.7	-0.6	-0.8	
- 19 3	54.3	55.5	62.8	57.5	0.1	0.4	0.7	0.4
+	52.6	53.4	59.9	55.3	-1.5	-1.7	-2.2	-1.8
1st deriv.					-0.8	-1.1	-1.5	
- 19 4	3.2	4.3	5.1	4.2	-1.1	-0.6	-0.8	-0.8
+	4.9	5.3	6.4	5.5	0.6	0.4	0.5	0.5
1st deriv.					0.9	0.5	0.7	
- 19 5	5	5.3	6.5	5.6	0.6	0.4	0.6	0.5
+	3.2	4.4	5.1	4.2	-1.2	-0.6	-0.8	-0.9
1st deriv.					-0.9	-0.5	-0.7	
- 19 6	52.6	53.4	59.9	55.3	-1.5	-1.8	-2.2	-1.8
+	54.3	55.4	62.8	57.5	0.1	0.3	0.7	0.4
2nd deriv.					-0.7	-0.8	-0.8	
- 19 6	52.6	53.4	59.9	55.3	-1.5	-1.8	-2.2	-1.8
+	54.3	55.4	62.8	57.5	0.1	0.3	0.7	0.4
1st deriv.					0.8	1.1	1.5	
- 20 1	4.4	4.8	6	5.1	0.1	-0.1	0.2	0.1
+	3.4	4.5	5.2	4.4	-0.8	-0.4	-0.6	-0.6
1st deriv.					-0.5	-0.2	-0.4	
- 20 3	52.8	53.8	60.7	55.8	-1.4	-1.3	-1.4	-1.3
+	54.1	55	62	57.1	0	-0.1	-0.1	-0.1
2nd deriv.					-0.7	-0.7	-0.8	
- 20 3	52.8	53.8	60.7	55.8	-1.4	-1.3	-1.4	-1.3
+	54.1	55	62	57.1	0	-0.1	-0.1	-0.1
1st deriv.					0.7	0.6	0.6	
- 20 4	3.4	4.5	5.2	4.4	-0.8	-0.4	-0.6	-0.6
+	4.3	4.8	5.9	5	0.1	-0.1	0.1	0
1st deriv.					0.5	0.2	0.3	
- 20 6	54.1	55	62	57	-0.1	-0.1	-0.1	-0.1
+	52.7	53.7	60.7	55.7	-1.4	-1.4	-1.4	-1.4

displacement, mode, N atom	A_{xx}	A_{yy}	A_{zz}	A_{iso}	ΔA_{xx}	ΔA_{yy}	ΔA_{zz}	ΔA_{iso}
2nd deriv.					-0.8	-0.8	-0.8	
- 20 6	54.1	55	62	57	-0.1	-0.1	-0.1	-0.1
+	52.7	53.7	60.7	55.7	-1.4	-1.4	-1.4	-1.4
1st deriv.					-0.6	-0.6	-0.6	
- 21 3	52.5	53.5	60.6	55.5	-1.7	-1.6	-1.5	-1.6
+	55.4	56.2	63.2	58.3	1.2	1.1	1.1	1.2
1st deriv.					1.4	1.4	1.3	
- 21 6	55.4	56.2	63.2	58.2	1.2	1.1	1.1	1.1
+	52.5	53.6	60.6	55.5	-1.6	-1.6	-1.5	-1.6
1st deriv.					-1.4	-1.4	-1.3	

References

1. E. S. Gore, D. H. Busch, *Inorg. Chem.*, 1973, **12**, 1.
2. B. Bosnich, M. L. Tobe, G. A. Webb, *Inorg. Chem*., 1965, **4**, 1109.
3. L. Prasad, S. C. Nyburg, A. McAuley, *Acta Cryst*., 1987, **C43**, 1038.
4. A. McAuley, T. Palmer, T. W. Whitcombe, *Can. J. Chem.*, 1993, **71**, 1792.
5. A. M. Funston, W. D. McFadyen, P. A. Tregloan, *Aust. J. Chem*., 2002, **55**, 535.
6. G. A. Bain, J. F. Berry, *J. Chem. Ed.*, 2008, **85**, 532-538.
7. G. M. Sheldrick, SADABS, Version 2.03; *Bruker Analytical X-Ray Systems*, Madison, WI, **2000**.
8. L. J. Farrugia, *J. Appl. Cryst*., 2012, **45**, 849-854.
9. R. E. Stratmann, G. E. Scuseria, M. J. Frisch, *J. Chem. Phys.*, 1998, **109**, 8218-8224.
10. M. J. Frisch, G. W. Trucks, H. B. Schlegel, G. E. Scuseria, M. A. Robb, J. R. Cheeseman, G. Scalmani, V. Barone, G. A. Petersson, H. Nakatsuji, X. Li, M. Caricato, A. V. Marenich, J. Bloino, B. G. Janesko, R. Gomperts, B. Mennucci, H. P. Hratchian, J. V. Ortiz, A. F. Izmaylov, J. L. Sonnenberg, D. Williams-Young, F. Ding, F. Lipparini, F. Egidi, J. Goings, B. Peng, A. Petrone, T. Henderson, D. Ranasinghe, V. G. Zakrzewski, J. Gao, N. Rega, G. Zheng, W. Liang, M. Hada, M. Ehara, K. Toyota, R. Fukuda, J. Hasegawa, M. Ishida, T. Nakajima, Y. Honda, O. Kitao, H. Nakai, T. Vreven, K. Throssell, J. A. Montgomery Jr., J. E. Peralta, F. Ogliaro, M. J. Bearpark, J. J. Heyd, E. N. Brothers, K. N. Kudin, V. N. Staroverov, T. A. Keith, R. Kobayashi, J. Normand, K. Raghavachari, A. P. Rendell, J. C. Burant, S. S. Iyengar, J. Tomasi, M. Cossi, J. M. Millam, M. Klene, C. Adamo, R. Cammi, J. W. Ochterski, R. L. Martin, K. Morokuma, O. Farkas, J. B. Foresman, D. J. Fox, Gaussian 16, Revision A.03, Gaussian, Inc., Wallingford CT, 2016.
11. (a) K. Raghavachari, J. S. Binkley, R. Seeger, J. A. Pople, *J. Chem. Phys.*, **1980**, *72*, 650-54; (b) P. J. Hay, *J. Chem. Phys.*, 1977, **66**, 4377-84.
12. A. D. Becke, *J. Chem. Phys*., 1993, **98**, 5648-52.
13. J. L. Pascual-Ahuir, E. Silla, and I. Tuñón, *J. Comp. Chem*., 1994, **15**, 1127-38.
14. R. Seeger, J. A. Pople, *J. Chem. Phys*., 1977, **66**, 3045-50.
15. F. Neese, *Wires Comput. Mol. Sci.*, 2012, **2**, 73-78.
16. V. Barone, Recent Advances in Density Functional Methods, Part 1 (ed. D. P. Chong), World Scientific, Singapore, 1995, p. 287.
17. (a) C. Angeli, R. Cimiraglia, S. Evangelisti, T. Leininger, J.-P Malrieu, *J. Chem. Phys.*, 2001, **114**, 10252−10264. (b) C. Angeli, R. Cimiraglia, J.-P. Malrieu, *J. Chem. Phys*., 2002, **117**, 9138−9153. (c) C. Angeli, M. Pastore, R. Cimiraglia, *Theor. Chem. Acc*., 2007, **117**, 743−754.
18. F. Neese, *J. Chem. Phys*, 2003, **119**, 9428-9443.
19. T. H. Dunning Jr., *J. Chem. Phys*.,1989, **90**, 1007.
20. V. Barone, M. Cossi, *J. Phys. Chem. A*, 1998, **102**, 1995.
21. N. F. Chilton, R. P. Anderson, L. D. Turner, A. Soncini, K. S. Murray, *J. Comput. Chem*., 2013, **34**, 1164-1175.
22. (a) A. Larson, V. Von Dreele, General Structure Analysis System (GSAS); Vol. MS- H805, **1994**. (b) B. H. Toby, *J. Appl. Crystallogr*., 2001, **34**, 210–213.
23. (a) G. Kresse, J. Hafner, *Phys. Rev. B*, 1993, **47**, 558–561. (b) G. Kresse, J. Hafner, *Phys. Rev. B*, 1994, **49**, 14251–14269. (c) Kresse, G.; Furthmüller, *J. Comput. Mater. Sci.*, 1996, **6**, 15–50.
24. G. Kresse, *Phys. Rev. B* 1999, **59**, 1758–1775.